Design and synthesis of fluorescent ligands for the detection of cannabinoid type 2 receptor (CB2R)

Design and Synthesis of Fluorescent Ligands for the Detection of Cannabinoid Type 2 Receptor (CB2R)

Francesco Spinelli,[a#] Roberta Giampietro,[a#] Angela Stefanachi,[a] Chiara Riganti,[b] Joanna Kopecka,[b] Francesca Serena Abatematteo,[a] Francesco Leonetti,[a] Nicola Antonio Colabufo,[a ,c] Giuseppe Felice Mangiatordi,[d] Orazio Nicolotti,[a] Maria Grazia Perrone,[a] José Brea,[f] María Isabel Loza,[f] Vittoria Infantino,[e] Carmen Abate,[a]* Marialessandra Contino[a]*

[a]Dipartimento di Farmacia-Scienze del Farmaco, Università degli Studi di Bari ALDO MORO, via Orabona 4, 70125, Bari Italy

[b]Dipartimento di Oncologia, Università degli Studi di Torino, via Santena 5/bis, 10126, Torino, Italy

[c]Biofordrug s.r.l., Spin-off dell'Università degli Studi di Bari ALDO MORO, Via Orabona 4, 70125 Bari, Italy

[d]CNR - Istituto di Cristallografia, Via Amendola, 122/o 70126 Bari, Italy

[e] Department of Science, University of Basilicata, 85100 Potenza, Italy.

[f] Innopharma Screening platform. BioFarma Research group. Center for Research in Molecular Medicine and Chronic Diseases (CIMUS), University of Santiago de Compostela, 15782, Santiago de Compostela, Spain.

[#]the two authors equally contributed to the paper

ABSTRACT

The Cannabinoid 2 receptor, CB2R, belonging to the endocannabinoid system, ECS, is involved in the first steps of neurodegeneration and cancer evolution and progression and thus its modulation may be exploited in the therapeutic and diagnostic fields. However, CB2Rs distribution and signaling pathways in physiological and pathological conditions are still controversial mainly because of the lack of reliable diagnostic tools. With the aim to produce green and safe systems to detect CB2R, we designed a series of fluorescent ligands with three different green fluorescent moieties (4-dimethylaminophthalimide, 4-DMAP, 7-nitro-4-yl-aminobenzoxadiazole, NBD, and Fluorescein-thiourea, FTU) linked to the the N1-position of the CB2R pharmacophore *N*-adamantyl-4-oxo-1,4-dihydroquinoline-3-carboxamide through

polymethylene chains. Compound **28** emerged for its compromise between good pharmacodynamic properties (CB2R K_i = 130 nM and no affinity *vs* the other subtype CB1R) and optimal fluorescent spectroscopic properties. Therefore, compound **28** was studied through FACS (saturation and competitive binding studies) and fluorescence microscopy (visualization and competitive binding) in engineered cells (CB2R-HEK293 cells) and in diverse tumor cells. The fluoligand binding assays were successfully set up, and affinity values for the two reference compounds GW405833 and WIN55,212-2, comparable to the values obtained by radioligand binding assays, were obtained. Fluoligand **28** also allowed the detection of the presence and quantification of the CB2R in the same cell lines. The interactions of compound **28** within the CB2R binding site were also investigated by molecular docking simulations, and indications for the improvement of the CB2R affinity of this class of compounds were provided. Overall, the results obtained through these studies propose compound **28** as a safe and green alternative to the commonly used radioligands for in vitro investigations.

KEYWORDS: Cannabinoid receptors, CB2R, fluorescent probes, CB2R fluorescent ligands, fluorescent competitive binding assay, flow cytometry study.

1.Introduction

Cannabinoid receptor subtype 2 (CB2R) is a G-protein-coupled receptor (GPCR) belonging to the EndoCannabinoid System (ECS) along with the cannabinoid receptor subtype 1 (CB1R). CB1R and CB2R are Gi proteins mainly differing for their tissue expression pattern [1-8]. Indeed, CB1R is physiologically localized in the Central Nervous System (CNS), in regions important for cognition, memory, motor activity (cortex, hippocampus, basal ganglia and cerebellum), and appetite (hypothalamus). A CB1R expression in peripheral organs (uterus and prostate) has also been reported [1-8]. On the other hand, in physiological conditions, CB2R is mostly localized in peripheral organs such as the immune system (macrophages and lymphocytes), tonsils, lymphnodes and spleen [1-8]. Neverthless, its overexpression is observed in neuroinflammation (activated microglia) [2, 9, 10], in neurodegenerative diseases [2, 11-17] and in different types of cancers [2, 17-25]. Unlike CB1R, CB2R activation does not lead to psychotropic effects, likely being CB2R expression negligible in neurons.

In the last two decades, CB2R modulation has disclosed many potential therapeutic effects, as the result of its pivotal role in cancer onset and progression and in neurodegeneration. Several types of tumors such as prostate, skin, liver, and breast cancers, overexpress CB2R with the expression level likely related to tumor aggressiveness [18-26]. In CNS pathological conditions, CB2R activation may induce neuronal survival acting on: i) modulation, migration and cytokine production from microglia and other invading immune cells [27-30]; ii) the inhibition of excitotoxicity, oxidative stress and apoptosis in neurons [30-33]; iii) the release of anti-inflammatory and pro-survival mediators from astrocytes [34,35].

However, CB2R distribution and its roles in physiological and pathological conditions are still controversial and no reliable tools (i.e. specific antibodies) are available to solve these issues.

Thus, starting from the overall reported CB2R upregulation in cancers and in the first phases of neuroinflammation, efforts are in progress to meet the need for CB2R imaging.

Unfortunately, few CB2R-targeting contrast agents were successful in the non-invasive Positron Emission Tomography (PET) imaging to detect the receptor ~~in cancers~~ [36-39] and only a limited number of studies has been carried out with other imaging techniques (Magnetic Resonance Imaging (MRI), ultrasound and optical imaging) [40,41]. Imaging techniques based on the fluorescent properties of either protein or their ligands are excellent biological approaches as they are able to provide a wealth of information about the protein under investigation. Fluorescence imaging is characterized by high resolution and sensitivity. Its main application is the receptor visualization that may serve as a valid method to identify CB2R pathways in physiological as well as pathological conditions. Additionally, fluorescence-based techniques have been employed as a low-cost alternative to classical radioligand-based assays. Besides that, other fluorescence advantages are safety, the high spatial resolution, the long shelf-life and the absence of radioactive decay, while the simultaneous use of different fluorescent probes may allow the detection of different targets in the same experiment [42].

The commonly adopted strategy in CB2R fluorescent ligands development is based on the linkage of the CB2R pharmacophore to a fluorescent moiety through different types of linkers. In 2005, Yates and coworkers [43] developed compound **1** (Fig. 1A), where the CB2R ligand scaffold was the 2-methyl-1-propyl-1*H*-indol-3-yl)-1-naphthalenylmethanone (JWH-015: K_i = 36 nM) connected to 7-nitrobenzoxadiazole (NBD) as fluorescent tag through a short acetamide linker [43,44]. This strategy was

unsuccessful as it led to a compound devoid of affinity vs CB2R [44]. Better results were obtained with compound **2** (NMP6) (Fig. 1A), where the CB2R ligand scaffold was a 6-methoxy-N-alkylisatin acylhydrazone [45] and NBD was used as the fluorescent tag. Compound **2** showed a moderate but strongly selective CB2R binding affinity (K_i = 387 nM) [45]. Bai and coworkers [46] followed the same strategy to develop Near-InfraRed (NIR) emitting probes as a new series of CB2R fluorescent agents that are more suitable for in vivo applicability (increased signal-to-noise ratio, improved sensitivity, reduced autofluorescence and light scattering, and deeper penetration). These new fluorescent compounds were based on the well-known CB2R antagonist **3** (SR144528) [47] functionalized with a diamino-hexane linking different NIR probes (Fig. 1B) [48-53]. Two other different CB2R pharmacophores based on quinolone and pyrazolpyrimidinone scaffolds, were also functionalized with NIR760 probe (Fig. 1C, compounds NIR760-Q **4** and NIR760-XLP6 **5**). However, all of these NIR-emitting molecules displayed moderate affinity towards the CB2R target [54,55].

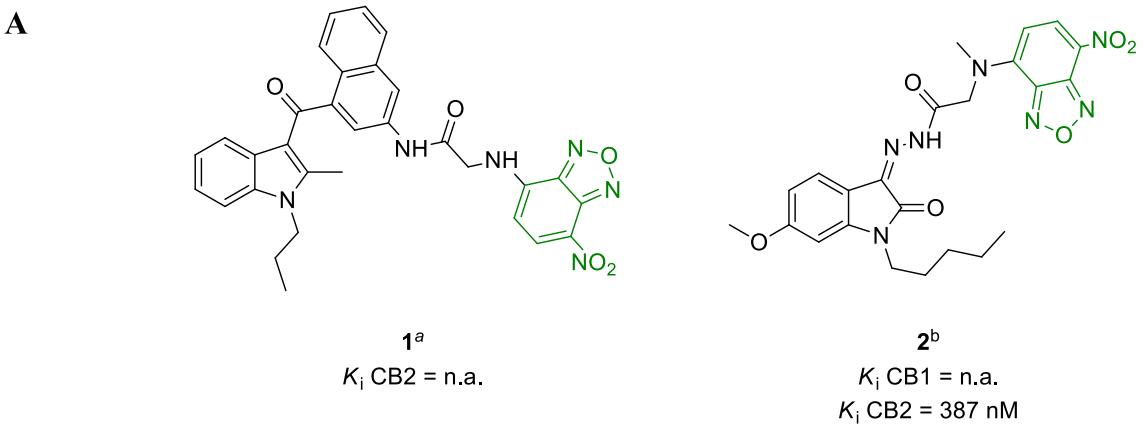

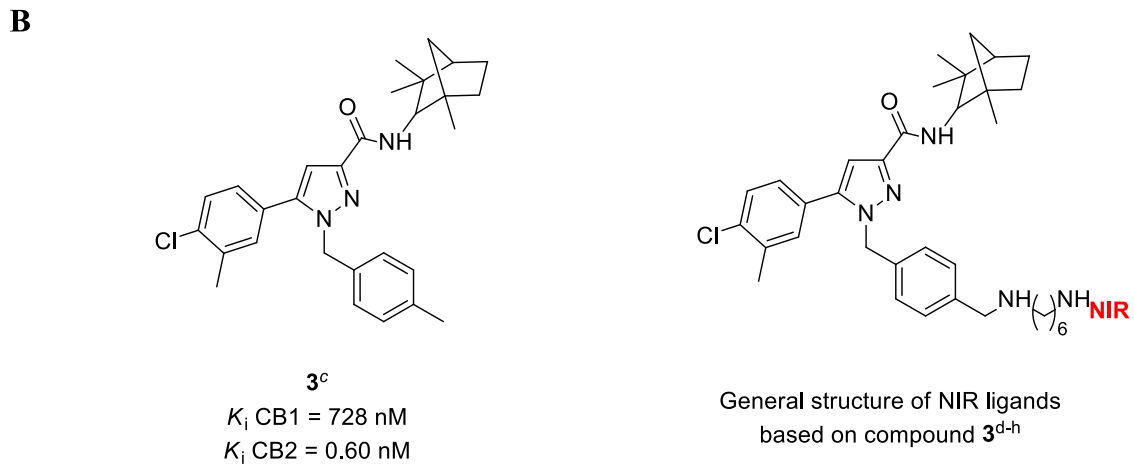

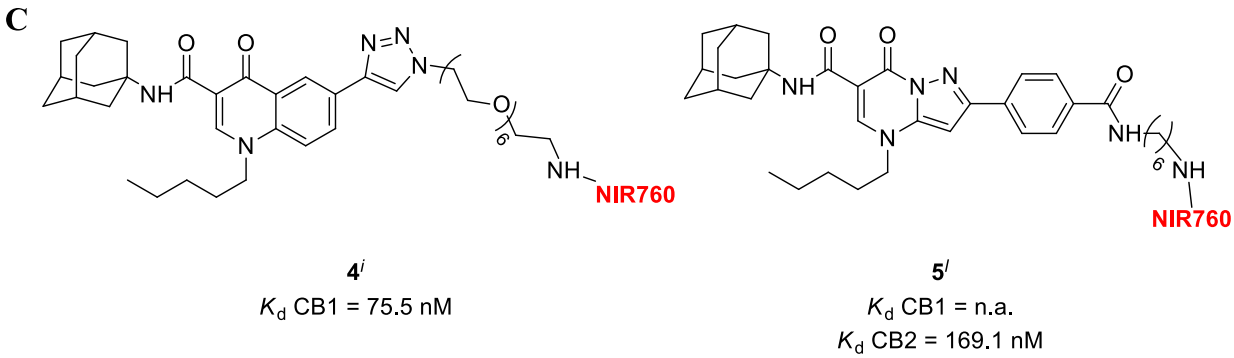

Fig. 1. 2D-structures of the most known CB2R fluorescent ligands. (A) Fluorescent derivative **1** and 6-methoxy-*N*-alkylisatin acylhydrazone-based fluorescent ligand **2**; (B) **3**, its near-infrared emitting derivatives (General Structure); (C) quinolone-based **4** and pyrazolpyrimidine-based **5** NIR760 fluorescent ligands. Binding data from reported references: [a] from ref. 43, [b] from ref. 46, [c]

from ref. 48, [d] from ref. 49, [e] from ref. 50, [f] from ref. 51, [g] from ref. 52, [h] from ref. 53; [i] from ref. 54, [l] from ref. 55; n.a., not active.

Following the same approach, among the diverse CB2R reported pharmacophores we selected the *N*-adamantyl-1-pentyl-4-oxo-1,4-dihydroquinoline-3-carboxamide scaffold (compound **6**, Figure 2) [56,57] and three different green fluorescent moieties: 1) 4-dimethylaminophthalimide (4-DMAP, moiety A in Fig. 2); 2) 7-nitro-4-yl-aminobenzoxadiazole (NBD, moiety B in Fig. 2); 3) Fluorescein-thiourea (FTU, moiety C in Fig. 2). The core structure of compound **6** was selected because of its excellent CB2R affinity and selectivity profile and for its ability to tolerate large aromatic substituents at the N_1-position [57], where we connected the fluorescent tags through a polymethylene linker (Fig. 2). Tags A and B have been widely employed with good success for the development of fluorescent ligands, because of their small sizes, that generally do not considerably alter the pharmacophore [58-62]. Tag C is usually reported as fluorescent tag in the development of fluoligands because of its high quantum yield, so that a series of fluorescein-bearing probes for diverse proteins have been developed and can be purchased from the chemicals' suppliers.

The length of the linker bridging the fluorescent tag and the pharmacophore was explored going from six- to twelve-methylene chains, in order to identify the optimal distance between pharmacophore and fluorescent tag for CB2R binding. For the fluorescein-bearing compounds (tag C), we only explored the six-methylene and ten-methylene linkers, in order to have a general indication about the possible fit of these ligands, whose interaction with the binding site may be not allowed because of the steric hindrance of the tag.

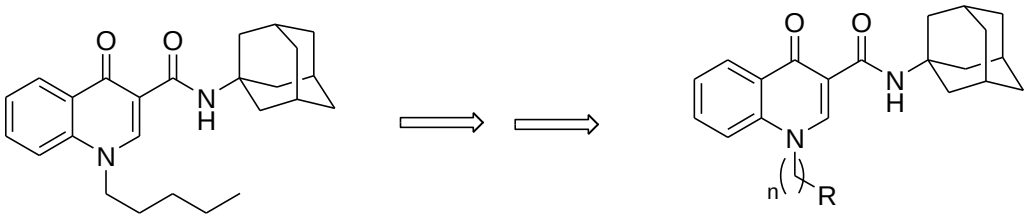

6

Fluorescent ligands' general structure

R =

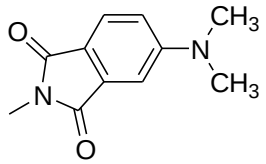

A

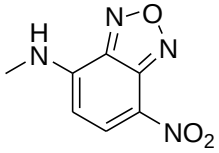

B

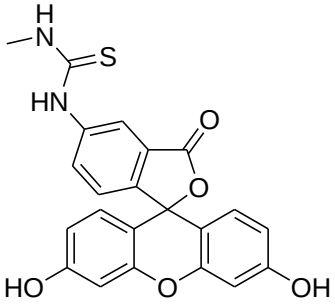

C

Fluorescent moieties

Fig. 2. Fluorescent ligands' general structure.

2. Chemistry

The synthesis of target compounds was accomplished as depicted in Schemes 1 and 2. 4-Oxo-1,4-dihydroquinoline core structure **7** was synthesized according to the published procedure (56). Compound **7** was alkylated with α,ω-dibromoalkanes under microwave irradiation affording the *N*-bromoalky-l,4-oxo-quinolines **8-11**. Reaction with NaN_3 at 60 °C in dry DMF gave the corresponding *N*-azidoalkyl derivatives **12-15**, whose ester function was hydrolyzed under basic condition to provide the corresponding carboxylic acids **16-19**. Activation of these acids with HBTU, as coupling reagent, in presence of DIPEA in dry DMF afforded adamantylamides **20-23** [57] which underwent Staudinger reaction with triphenylphosphine in dry MeOH to obtain primary amines **24-27** [63] (Scheme 1).

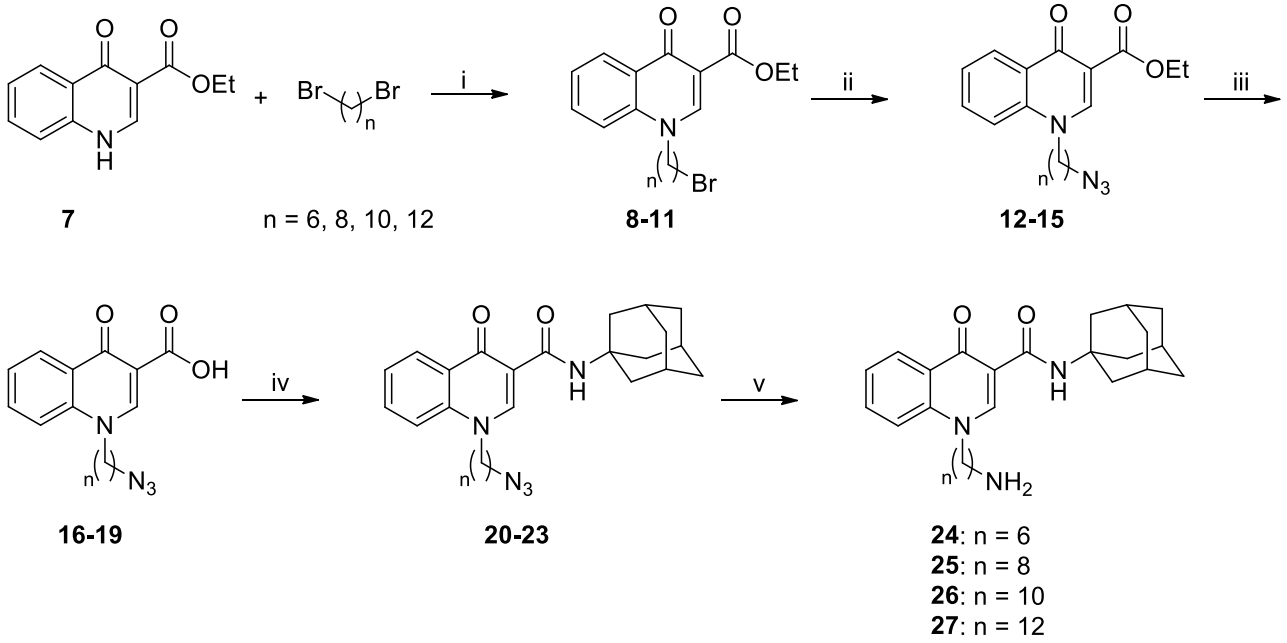

Scheme 1. Synthesis of intermediates 8-27. Reagents and conditions: (i) K_2CO_3, CH_3CN, MW, 160 °C, 45 min; (ii) NaN_3, dry DMF, 60 °C, 24 h; (iii) NaOH 2 N, EtOH, rt, 4 h; (iv) 1-adamantylamine, HBTU, DIPEA, dry DMF, rt, 20 h; v) Ph_3P, dry MeOH, 80 °C, 1 h.

Final fluorescent compounds **28-31** were afforded by reaction between the appropriate amine among **24-27** and 4,4-dimethylaminophthalic acid previously activated with HBTU in presence of DIPEA [64]. Final fluorescent compounds **32-35** were obtained by aromatic nucleophilic substitution between amines **24-27** with 4-chloro-7-nitrobenzoxadiazole in EtOH. Finally, compounds **36** and **37** were synthesized by addition

of amines **24** and **26** to the commercially available fluorescein isothiocyanate (FITC) in the presence of DIPEA (Scheme 2).

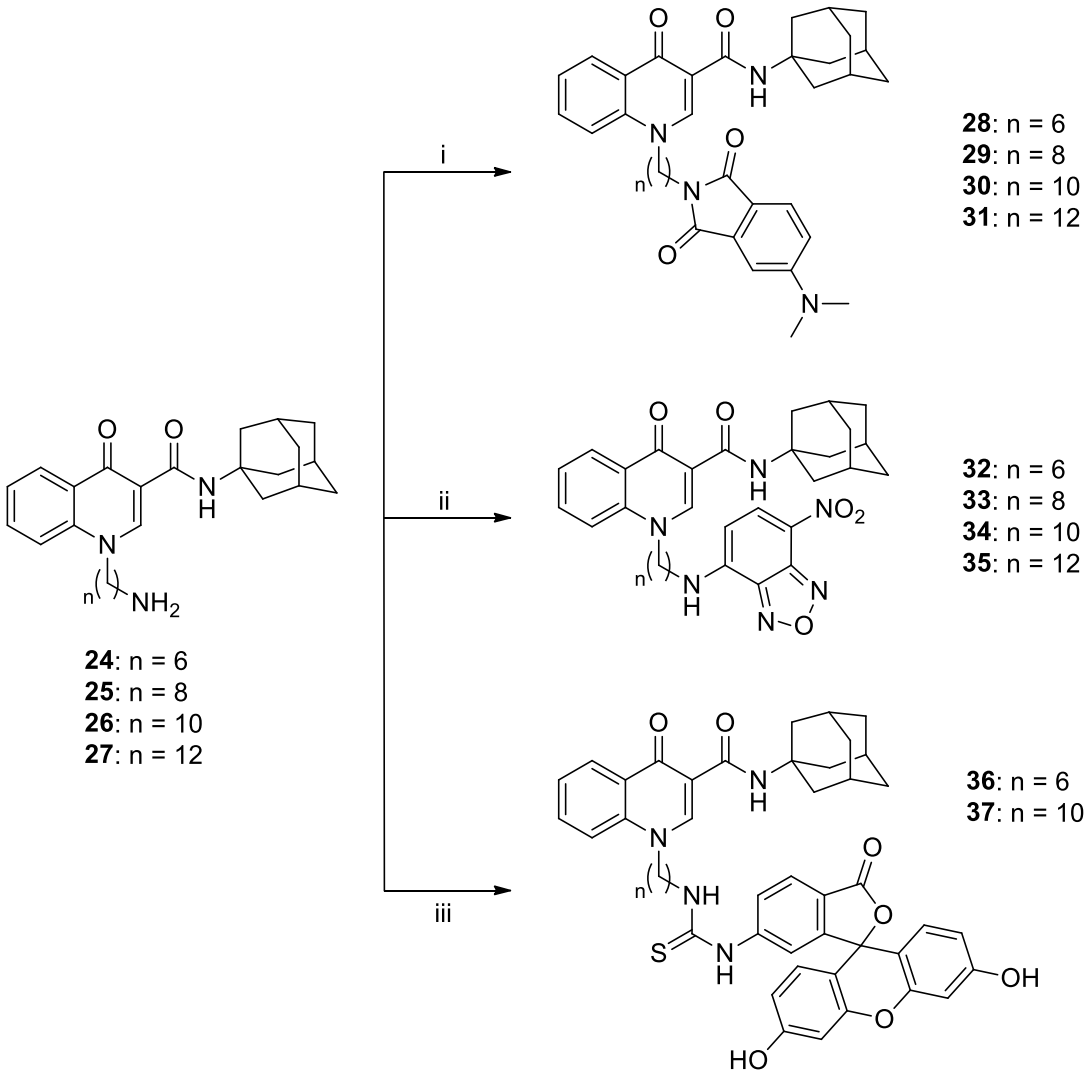

Scheme 2. Synthesis of fluorescent compounds 28-37. Reagents and conditions: (i) 4,4-dimethylaminophthalic acid, HBTU, DIPEA, dry DMF, rt, 20 h; (ii) 4-chloro-7-nitrobenzoxadiazole, EtOH, rt, 4 h; (iii) fluorescein isothiocyanate, DIPEA, dry DMF, rt, 1 h.

3. Results

3.1 Radioligand binding assay at CB2 and CB1 receptor subtypes

All the synthesized compounds were tested for their binding affinity towards CB1R and CB2R subtypes. Their *K*i values, together with those of compound **6** and reference ligands are listed in Table 1. The binding assays have been performed on a cell model (HEK293 cells overexpressing human CB2R) which was developed as CB2R model and validated in our laboratory (see Supporting Information).

Table 1

CB2R and CB1R affinity values for compounds **28**-**37**.

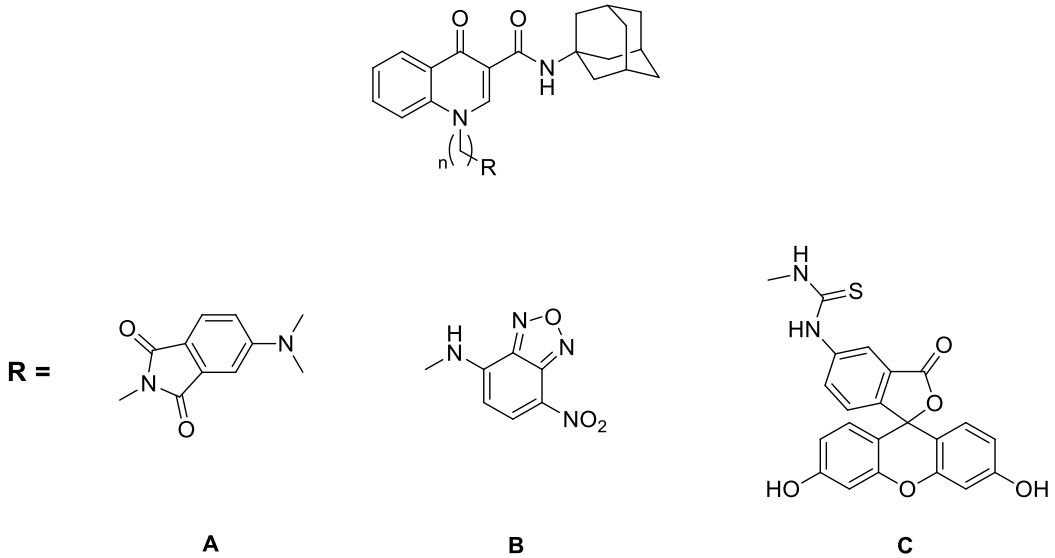

Compounds	R	n	CB2R[a]	CB1R[a,b]
			*K*i ± SEM, nM	
28	A	6	130±7	14%
29	A	8	13%[b]	36%
30	A	10	13%[b]	4%
31	A	12	2%[b]	21%
32	B	6	1920±30	17%
33	B	8	800±10	6%
34	B	10	2550±150	12%
35	B	12	6950±950	11%
36	C	6	2900±700	24%[e]
37	C	10	2800±300	17%[e]
6			0.68±0.14[c]	42.1[e]

GW405833			3.92±0.80[c]	-
R-(+)-WIN55,212-2			2.37[d]	-
Surinabant			-	3.8

[a]Data represent mean values of n ≥ 3 separate experiments in duplicate (± SEM for CB2R). [b] Percentage of displacement at the concentration of 1 μM.[c]The binding affinities of reference compounds were evaluated in parallel with test compounds under the same conditions.[d]Value from reference 66.[e] Percentage of displacement at the concentration of 10 μM.[e] Value from reference 57.

None of the novel compounds showed affinity for the CB1R with only a low percentage of the radioligand displacement at high concentration of the target compound (10^{-5} M or 10^{-6} M), differently from compound **6** displaying a moderate CB1R affinity (K_i = 42.1 nM) (57). The insertion of the fluorescent moieties A, B or C at the terminal position of the N_1-alkyl linker at the 4-oxo-1,4-dihydroquinoline scaffold was strongly detrimental for CB2R binding compared to lead compound **6** (K_i= 0.68 nM for compound **6** *vs* K_i values close to 1000 nM for almost all the newly synthesized compounds). The highest affinity for CB2R was shown by **28**, bearing the hexamethylene linker between the fluorescent moiety A (4-DMAP) and the CB2R pharmacophore (CB2R K_i = 130 nM; CB1R > 1000 nM). In this series of 4-DMAP-bearing compounds (**29-31**), the elongation of the hexamethylene linker led to a complete loss of CB2R affinity (CB2R K_i > 1000 nM). On the other hand, a different behavior was observed in the NBD-bearing series (**32**-**35**), where the best CB2R affinity value was observed for compound **33**, carrying an octamethylene-chain (CB2R K_i = 800 nM), instead of a six-methylene linker as in compound **32** (CB2R K_i = 1920 nM). The binding strongly decreased for the compounds bearing longer methylene chains as for compounds **34** and **35** (CB2R K_i = 2550 nM and 6950 nM, respectively). The notable difference in the CB2R affinity between the six-methylene bearing compounds of the 4-DMAP (i.e. **28**) and the NBD -bearing series (i.e. **32**), suggests a diverse binding mode within the CB2R binding site.

In the FTU-bearing compounds, poor CB2R affinity was found either in the six-methylene or in the ten-methylene bearing compounds (K_i CB2R = 2900 nM and 2800 nM for **36** and **37**, respectively).

All in all, the results from the binding assays suggest that modifications of the scaffold of compound **6** through the elongation of the pentyl chain to six till twelve –methylene chain carrying a moiety at the ω-position, strongly decreases the CB2R binding irrespective of the size of such a moiety. These results are in line with the literature data, indicating that the decoration of diverse CB2R pharmacophores with fluorescent

tags at diverse positions, leads to a drop in the CB2R binding affinity. In our series, only the six-methylene DMAP bearing derivative **28** is endowed with an appreciable binding at the CB2R, with one of the highest affinities among the fluorescent CB2R ligands known. Therefore, compound **28** emerged as worthy of further investigations.

3.2 Fluorescent properties

The fluorescent properties of the final compounds are listed in **Table 2** where the maximum excitation and emission wavelengths (λ_{ex} and λ_{em}, respectively) for each compound in organic solvents ($CHCl_3$, DMSO, and EtOH) and in aqueous solution (PBS buffer) at the concentration of 10^{-5} M are reported.

Table 2.

Fluorescent properties for compounds **28-37**.

Cmp	R_2	n	$CHCl_3$		DMSO		EtOH		PBS[a]	
			λ_{ex}	λ_{em}	λ_{ex}	λ_{em}	λ_{ex}	λ_{em}	λ_{ex}	λ_{em}
28	A	6	339	504	400	534	395	544	400	520
29	A	8	393	502	400	516	399	544	405	512
30	A	10	330	504	400	516	396	548	403	504
31	A	12	320	496	400	514	396	544	340	502
32	B	6	339	526	474	546	468	536	490	560
33	B	8	467	524	463	544	468	534	498	558
34	B	10	467	528	455	544	468	534	483	538
35	B	12	467	524	453	542	468	536	491	554
36	C	6	330	540	520	540	487	540	497	540
37	C	10	330	540	520	540	488	540	495	540

The 4-DMAP-bearing compounds **28-31** displayed λ_{ex} at ≈ 400 nm and the corresponding λ_{em} in the 500-550 nm range, depending on the solvent. The NBD-bearing compounds **32-35** showed a λ_{ex} shifted towards higher wavelengths (≈ 460 nm) compared to the 4-DMAP bearing compounds, and λ_{em} in the 520-560 range, depending on the solvent. The FTU-bearing compounds **36** and **37** showed a λ_{ex} shifted towards higher wavelengths (≈ 520 nm) compared to the 4-DMAP and NBD -bearing derivatives and λ_{em} in the 540 nm range. Overall, the calculated λ_{ex} and λ_{em} for all the novel fluorescent compounds were in accordance with the properties conferred by the insertion of the specific fluorescent moiety. The fluorophores herein used are known to be 'environment sensitive', as they display sensitivity to the local environment polarity. In

particular, 4-DMAP and NBD exhibit low fluorescence emission intensity in aqueous solution but become highly fluorescent in nonpolar solvents or when bound to a hydrophobic site in protein or membranes [65]. This behavior was confirmed for all the NBD-bearing compounds, that displayed high fluorescence emission intensity in all the organic solvents ($CHCl_3$, DMSO, and EtOH) at the lowest tested concentration (10^{-6} M), and a barely detectable fluorescence in PBS at the highest tested concentration (10^{-5} M). Surprisingly, a different behavior was recorded with 4-DMAP-bearing compounds **28**-**31** that exerted high fluorescence emission intensity both in organic and aqueous solvents ($CHCl_3$ and PBS), but a barely detectable fluorescence in the other organic solvents (DMSO and EtOH) at a concentration of 10^{-5} M. This behavior may suggest a different folding of the 4-DMAP bearing compounds compared to the NBD, which may be responsible of such particular fluorescent properties. FTU-bearing compounds displayed high fluorescence emission intensity in EtOH, PBS and DMSO, and a barely detectable fluorescence in $CHCl_3$ at the highest tested concentration (10^{-5} M). Overall, despite an affinity 200-fold lower than **6**, compound **28** is one of the highest affinity CB2R fluorescent ligands known in the literature, to the best of our knowledge. These pharmacodynamic properties combined with the optimal fluorescent spectroscopic properties (good Stokes shift and high fluorescence emission in organic and aqueous solutions, Fig. 3) make **28** a valuable tool to be investigated in CB2R related studies.

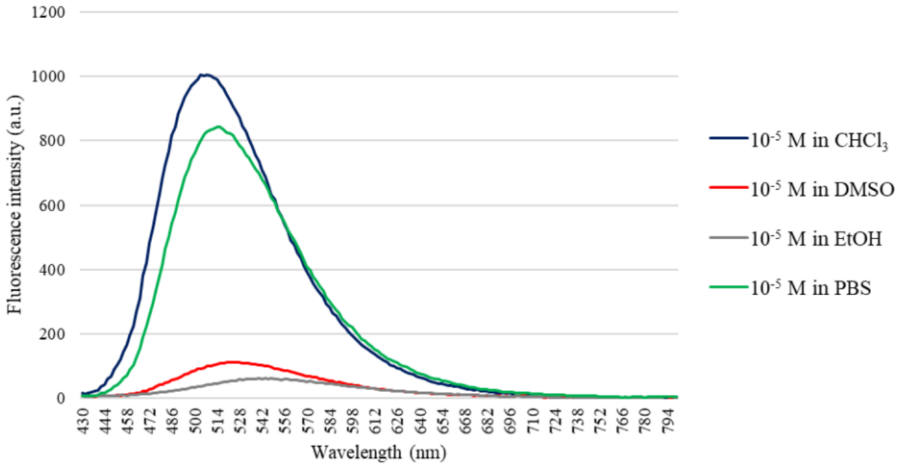

Fig. 3. Emission spectra of compound **28** in organic solvents ($CHCl_3$, DMSO, EtOH) and aqueous solution (PBS) at a concentration of 10^{-5} M. Excitation wavelength was 400 nm.

With this aim in mind, compound **28** was used for preliminary investigations through flow-cytometry analysis and fluorescence imaging experiments in HEK293 CB2R-overexpressing cells and in different types of tumour cells.

3.2 Cytotoxicity Study of compound 28

Compound **28** cytotoxicity has been assayed in all the cell lines where it was tested as fluoligand, (our CB2R-HEK293- cell model, and the selected cancer cell types human colon adenocarcinoma HT29 and their doxorubicin-resistant counterpart HT29-dx cells, human breast adenocarcinoma MCF7 and their doxorubicin-resistant counterpart MCF7-dx cells, pancreatic cancer PANC1, prostate cancer PC3 cell lines) in order to determine its potential application as a probe in living cells. Fluoligand **28** displayed low cytotoxicity in all the cells at 24 h demonstrating its suitability as fluorescent probe in the living cells imaging technique. A table showing the cytotoxicity of compound **28** in all the studied cell lines is reported in the supporting information.

3.4 Fluorescence-activated cell sorting (FACS) analysis

Flow cytometry analysis was performed in order to candidate compound **28** as a potential tool for:

1. Fluorescent-based competition binding assays (replacing the radioligand with the fluorescent ligand) as greener and safer alternative to the classical radioligand-based binding techniques;

2. The detection of CB2Rs in specific cell populations.

If **28** results a sensitive and specific ligand for CB2R, it could be a potentially useful tool used to investigate the signaling pathways regulated upon CB2R binding in future studies.

To establish the optimal conditions of **28** binding, a preliminary analysis was performed in CB2R-HEK293 cells, incubated with **28** at the concentrations of 0, 0.01 nM, 0.1 nM, 1 nM, 10 nM, 100 nM, 1 μM, 10μM, for 30, 60, 90, 120, 180 min. We found an appreciable fluorescence after 90 min of incubation, not at earliest time points. At 90 minutes, 0.01 nM, 0.1 nM, 1 nM of **28** did not produced a fluorescent signal significantly different from untreated, taken as cell autofluorescence. With 10 nM of **28** the fluorescent signal was higher

($p<0.02$) than in untreated cells; with 100 nM and higher concentrations of **28** the fluorescent signal was markedly different from the unlabeled cells ($p<0.001$). (data not shown) We thus identified the concentration of 100 nM od 28, with an incubation time of 90 min, as the most suitable condition for binding srudies.

3.4.1 Competitive binding assay of CB2R reference compounds with 28 as fluo-ligand

In order to validate **28** as fluoligand in a competitive binding assay, the two CB2R reference compounds *R*-(+)-WIN55,212-2 and GW405833 were tested.

Two complementary displacement analyses were set up:

1) A fixed concentration of the fluoligand **28** (100 nM) was displaced by increasing concentrations of the reference compounds (0.01nM-10μM) (fluo-competition binding assay to measure the IC_{50} of the two reference compounds);

2) A fixed concentration of the studied reference compound (10 μM) was challenged with increasing concentrations of **28** (1nM-10 μM) (displacement assay to confirm the interaction with CB2R site).

From the first setting of experiments, the IC_{50} values were measured and the results were perfectly comparable to the K_i values from the radioligand competition binding assays for both the reference ligands. The IC_{50} values experimentally obtained for both the reference compounds *via* the fluo-binding and the K_i values [66] derived from the competition binding assay with radioligand are reported in Table 3. The fluo-binding competition curves for (+)-WIN55,212-2 and GW405833 are depicted in Fig. 4. The results herein obtained suggest that compound **28** is a useful tool for the evaluation of the affinity of compounds vs CB2R in this engineered cell model.

Table 3. Affinity values *vs* CB2R of two CB2R reference compounds by competition binding assay performed by FACS (IC_{50}) or radioligand binding assay (K_i). IC_{50} values are the mean ± SEM of two experiments performed in triplicate.

Reference compounds	IC_{50}±SEM, nM	K_i, nM[a]
WIN55,212-2	1.2±0.20	2,37
GW405833	2.0±0.38	3.92

[a] K_i values reported in ref 66.

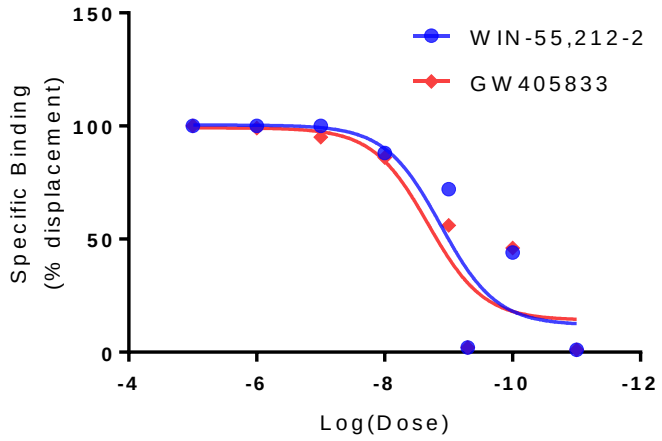

Fig. 4. CB2R competition binding assay with **28** 100 nM as probe by FACS: curves of CB2R reference compounds WIN-55,212-2 and GW405833 on CB2R-HEK293 stably transfected cells.

3.4.2 Saturation binding assay on CB2R-HEK293 cells with 28 as fluoligand

The selected clones of cells overexpressing CB2R after western blot analysis were validated by saturation binding assay with radioligand using the CBR agonist radioligand [^{3}H](-)-cis-3-[2-hydroxy-4-(1,1-dimethylheptyl)phenyl]-trans-4-(3-hydroxypropyl)cyclohexanol (CP55,940, PerkinElmer Italia SPA, Milano, Italy) as radioligand and GW405833 as reference compound. Data were analyzed using GraphPad Prism Version 7 (San Diego, CA, USA) and a K_d = 1.5 nM ([^{3}H]CP55,940 at CB2) and a B_{max} of 1.63 pmol/mg of protein were obtained (as depicted in Fig. S1, Supporting Information). The K_i observed for the CB2R reference compound GW405833 was consistent with what previously reported in the literature [66].

In order to define the K_D value of the fluoligand, a fluo-saturation analysis has been performed in vitro in our HEK293 cells overexpressing CB2R, by increasing the concentration of the fluoligand **28** (ranging from 0.01 nM to 25 μM) in the absence and in the presence of a fixed dose of the CB2R reference compound GW405833 (10 μM). The results depicted in Fig. 5 show a K_D of 44 nM for **28** and a B_{max} of 3 pmol/mg of

protein. Immunoprecipitation analysis was used to correlate RFU with CB2R protein amount and to normalize to cell proteins. Representative dose-dependence associated fluorescence curves of **28**, competition binding and saturation binding assays in HEK293-CB2R expressing cells are reported in Supporting Information Fig. S2. Wild-type HEK293 cells, that do not express CB2R, are included as internal control. The absence of fluorescence in wild-type HEK293 cells indicated the specificity of **28** binding to CB2R.

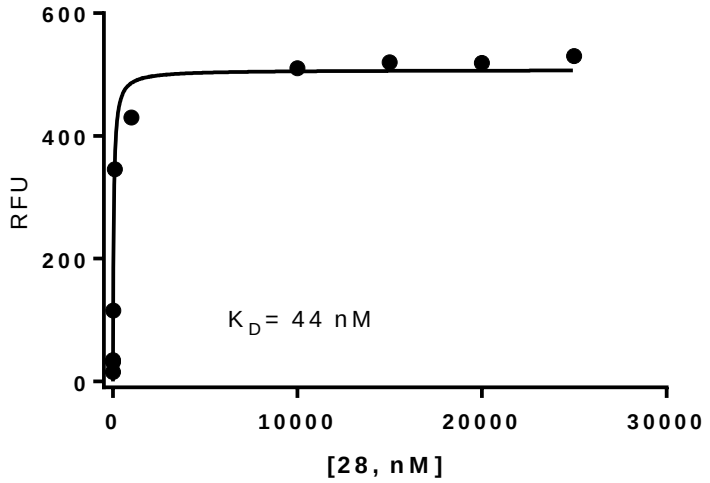

Fig. 5. In vitro CB2R Fluo-saturation binding assay of **28** in HEK293-CB2R cells. Specific binding data are represented as RFU (y-axis) and **28** concentration (x-axis). Data on the y-axis are measured by subtracting the non specific binding (obtained in the presence of the not fluorescent ligand GW405833 10μM) from the total binding (**28** 100 nM alone). The dissociation constant K_D and the receptor density B_{MAX} were measured by the nonlinear fitting of the specific binding vs **28** concentration using Prism software.

3.4.3 Saturation binding assay on tumour cells with 28 as fluoligand

Different human cancer cell lines (prostate cancer PC3, pancreatic cancer PANC1, colon adenocarcinoma HT29, breast adenocarcinoma MCF7 cells, glioblastoma U87-MG,–osteosarcoma U-2OS) were selected to test **28** as CB2R fluo-probe and the CB2R reference compound GW405833 as displacing agent. These cell lines were chosen since CB2R expression was already reported in the literature [67-78]. Moreover, two

resistant counterparts (MCF7-DX and HT29-DX) were also tested to investigate a possible different expression of CB2R between chemosensitive and chemoresistant cells. The presence of CB2R is confirmed in all the cells but the levels (represented by the specific binding measured as fluorescence value) are highly variable. As depicted in Fig. 6, the highest content of CB2R was observed in HT29-DX cells (100-fold more than the control cells, represented by HEK293 wild type cells), while PANC1 cells displayed the lowest expression of the receptor (5-fold more than the control cells). All of the other cell lines showed a comparable high amount of CB2R (around 20-fold more than the control cells). No significant difference was observed between MCF7 and the resistant counterpart MCF7-DX, although the latter expressed more CB2R than the former. By contrast, a significant difference was observed between HT29 and the resistant counterpart HT29-DX, with a 5-fold higher expression in the resistant one (Fig. 7). These data suggest that CB2R levels on cell surface are higher with the increase of resistance. The higher resistance of HT29-DX (adapted to survive in a medium containing 100 nM doxorubicin) compared to HT29, and the lower resistance of MCF7-DX (adapted to survive in a medium containing 40 nM doxorubicin) compared to MCF7 cells may explain the significant differences in CB2R levels in the more resistant cells HT29-DX *vs* HT29 cells, compared to the less resistant MCF7-DX *vs* MCF7 cells. This observation is worthy of further investigation.

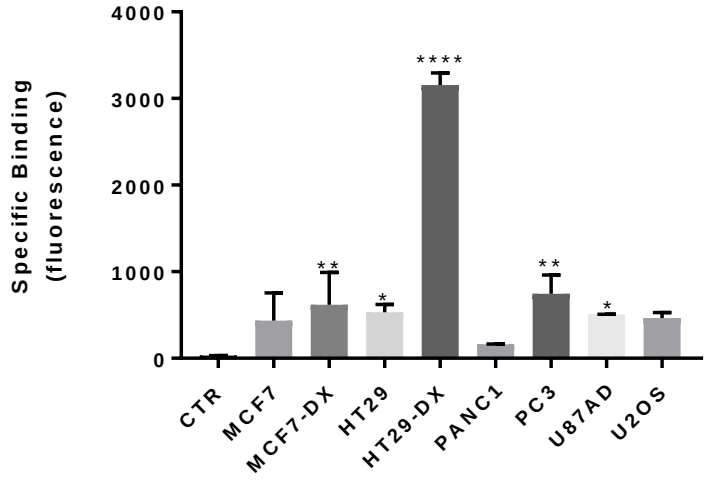

Fig. 6. CB2R specific binding comparison between different tumour cells performed by FACS with 100 nM **28** as CB2R fluo-probe and 10μM GW405833 as CB2R selective displacing agent. Each bar represents the mean ± SEM of two experiments performed in triplicate. One-way ANOVA analysis: *$p < 0.05$, **$p < 0.001$, ****$p < 0.0001$, *vs* control HEK293 cells.

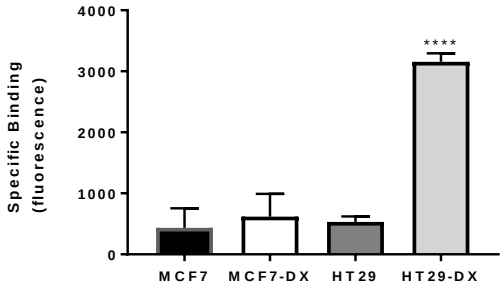

Fig. 7. CB2R specific binding comparison between MCF7 and HT29 cells and the resistant counterparts MCF7-DX and HT29-DX. The assay has been performed by FACS with 100nM **28** as CB2R fluo-probe and 10μM GW405833 as CB2R selective displacing agent. Each bar represents the mean ± SEM of two experiments performed in triplicate. One-way ANOVA analysis: ****$p < 0.0001$ *vs* HT29 cells.

3.5 Saturation binding assay with radioligand in selected tumor cells

In order to compare the findings obtained with our fluorescent probe **28**, with the commonly employed radioligand binding experiments, saturation binding assays with radioligand were performed in the most representative cancer cell lines as observed by fluorescent assays with **28** (MCF7-DX and HT29-DX and their wild-type counterpart MCF7 and HT29 and PC3 displaying the highest and PANC1 displaying the lowest amount of CB2R). Although no specific binding was detected in PANC1 cells and in none of the studied cell lines a high specific binding was observed (ranging from 20% to 40%), a significative difference between MCF7 and MCF7-DX cells (CB2R almost 2-fold more expressed in latter) (Fig 8A) and HT29 and HT29-DX cells (CB2R almost 10-fold more expressed in the latter) (Fig 8B) was detected, in agreement with the results from the fluoligand saturation binding assays. We may speculate that the paucity of the CB2R physiologically present in the above cell lines may be responsible of the low binding specificity detected through radioligand binding.

A

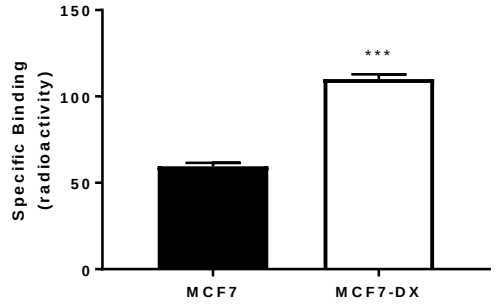

B

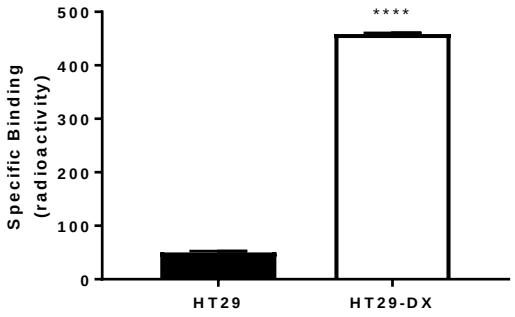

Fig. 8. (A) CB2R specific binding comparison between MCF7 cells and the resistant counterparts MCF7-DX cells performed by radioligand binding assay with 0.01 nM CP55,940 as CB2R probe and 10 μM GW405833 as CB2R selective displacing agent. (B) CB2R specific binding comparison between HT29 cells and the resistant counterparts HT29-DX cells performed by radioligand binding assay with 0.5 nM CP55,940 as CB2R probe and 10 μM GW405833 as CB2R selective displacing agent. Each bar represents the mean ± SEM of two experiments performed in triplicate. One-way ANOVA analysis: ***$p < 0.001$ vsMCF7 cells, ****$p < 0.0001$ vs HT29 cells.

3.5.1 Competitive binding assay of CB2R reference compound GW405833 with 28 as fluoligand in the selected tumour cell lines

As depicted, in Table 4, IC_{50} value for the CB2R reference compound GW405833 was also detected in the cancer cell lines above mentioned and are consistent with the value observed in our CB2R cell model (HEK293-CB2R cells). The results herein obtained suggest that compound **28** is useful for the evaluation of the affinity of compounds towards CB2R not only in cell models overexpressing CB2R (i.e. CB2R-HEK293), but also in tumor cells physiologically expressing CB2R.

Table 4.

IC_{50} value for the CB2R reference compound GW405833 in the different cell line by FACS using **28** 100nM as CB2R fluorescent probe. Each value represents the mean ± SEM of two experiments performed in triplicate.

Tumour cell lines	**IC_{50}±SEM, nM**
Human pancreatic cancer cell line PANC1	1.6±0.30
Human Bone Osteosarcoma Epithelial Cells U2OS	1.4±0.24
Human colon cancer cell line HT29	1.4±0.02
HT29-DX	1.1±0.20
Human glioblastoma U87AD	2.6±0.48
Human prostate cancer cell line PC3	0.55±0.31
Human cannabinoid receptor type 2 (CB2) expressing Human embryonic kidney 293 cells, CB2R-HEK293	2.0±0.38
Human embryonic kidney 293 cells, HEK293-wt	Nd
Human breast cancer cell line MCF7	2.4±1.04
MCF7-DX	2.8±0.65
Nd: not detected since the CB2R is not expressed in the cell line	

3.6 Fluorescence Microscopy studies with 28

The characterization of **28** as fluorescent probe for CB2R visualization was also deepened by immunofluorescence experiments through High-content Imaging System (PerkinElmer Operetta).

Firstly, CB2Rs were visualized incubating CB2R-HEK293 with anti-CB2R mouse monoclonal antibody conjugated with Alexa Fluor® 594 (Fig. 9). DAPI was used to visualize the nucleus.

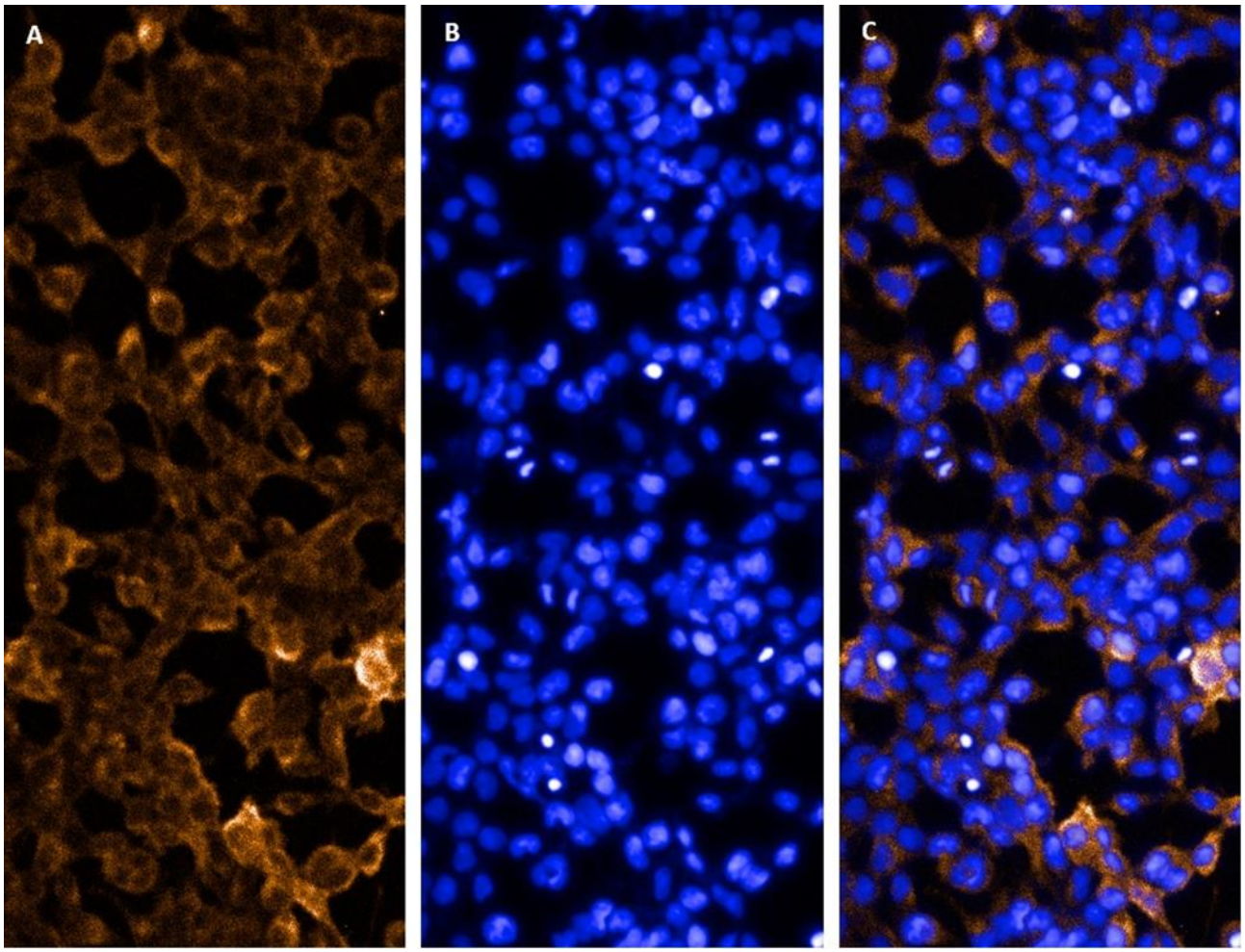

Fig. 9. PerkinElmer Operetta images (20 X magnification) acquired from anti-CB2R mouse monoclonal antibody conjugated with Alexa Fluor® 594 channel (A); DAPI (B); the merged image of CB2-R and DAPI (C).

Then, the ability of **28** to enter into the cells and accumulate at the level of the cytoplasm and plasma membrane (where CB2R is expressed) was verified (Fig. 10). Syto85 was used to visualize the nucleus. In this experiment DAPI has been substituted with Syto85 because of an overlapped emission wavelength with **28**. The same assay was conducted by using HEK293 wild-type cell line and, as expected, **28** fluorescence was not detected due to the absence of CB2R (data not shown).

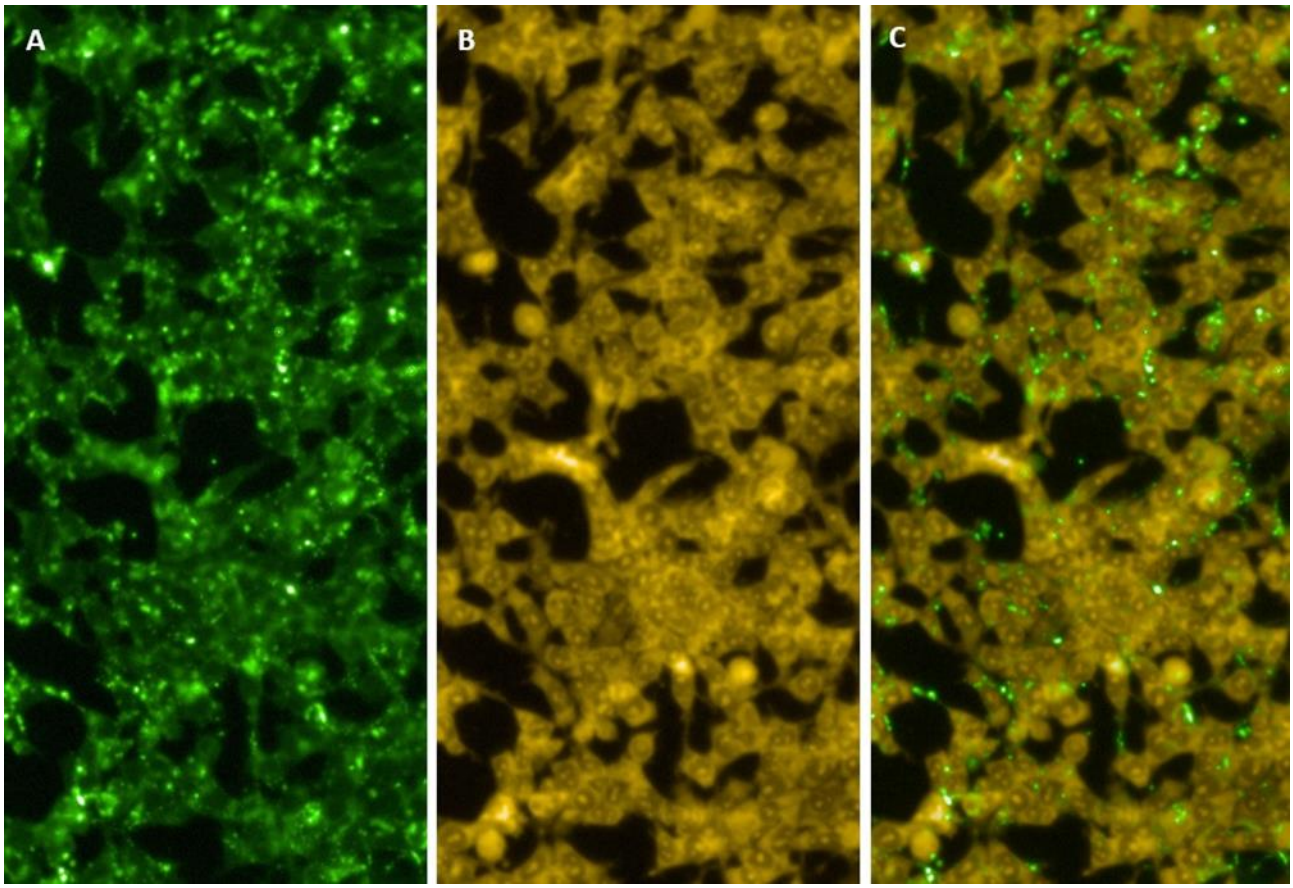

Fig. 10. PerkinElmer Operetta images (20 X magnification) acquired from **28** channel (A); Syto™85 (B); the merged image of **28** and Syto™85 (C).

Moreover, in order to test **28** as probe in a fluo-competition binding assay through the High-content Imaging System, different concentrations of **28** (0.1µM -50µM) were assayed. The fluorescence intensity emission was directly proportional to the increase in concentrations of **28**, revealing the specificity of this compound for the CB2R. The optimal fluoligand concentration was 15 µM because at 30 µM and 50 µM a huge fluorescence emission was detected indicating an off-sites binding (Table 6).

Table 6.

Mean fluorescence intensity emissions (f.u.) of 28 in CB2R-HEK293 quantified by Harmony.

[28], µM	f.u.
0	**39**
0.1	**39**
1	**40**
5	**57**
10	**84**
15	**97**
30	**2598**
50	**4830**

Hence, 15 µM was chosen as the concentration of **28** to perform the competition fluorescent binding assay with different GW405833 doses (0.01 nM-10 µM).

As reported in Fig. 11, the administration of GW405833 to CB2R-HEK293 in the presence of a fixed concentration of compound **28** (15 µM) determined a dose-dependent decrease in fluorescence units. This result indicates a displacement of the fluo-ligand by GW405833, that reached the 48% at the highest concentration (10 µM). The low displacement percentage is probably due to the high dose of **28** used in this kind of setting.

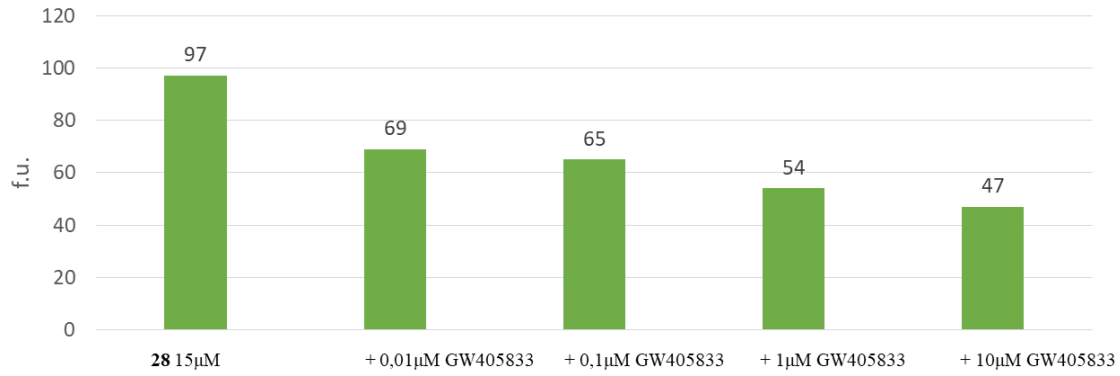

Fig. 11. Displacement (measured as fluorescent arbitrary unit) of the CB2R fluorescent probe **28** 15 μM alone and in the presence of different concentration (0,01-10μM) of the CB2R "cold" ligand GW405833.

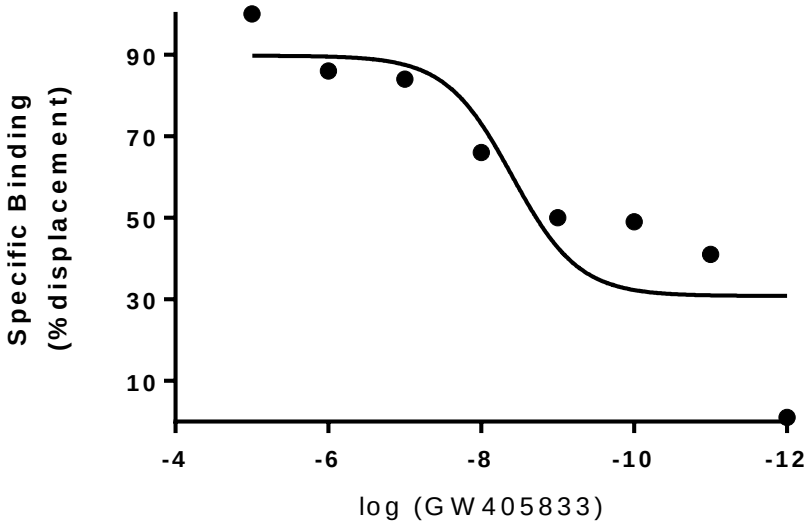

Fig. 12. CB2R competition binding curve of GW405833 (0.01 nM-10 μM) with **28** 15 μM in CB2R-HEK293- stably transfected cells.

In Fig. 12, the competition binding curve of the reference compound GW 405833 is depicted. The IC_{50} value of GW405833 obtained from the competition binding by high content technology is 3.94 nM, a value that can be superimposed to the value measured in radioligand binding assay (K_i = 3.92 nM). The results herein obtained elect **28** as a possible fluorescent alternative to the commonly used radioligand assay to detect the CB2R affinity.

3.7 Molecular docking simulations

With the aim of getting insights into the molecular interactions established by our fluorescent ligands within the binding site of CB2R, we carried out molecular docking simulations. It should be noted that performing robust docking simulations is nowadays possible due to the recent release of the first X-ray structure of CB2R in complex with an antagonist at 2.8 Å resolution (PDB code: 5ZTY, 79). In particular, we focused

our attention on two compounds, namely **28**, the most active derivative of our panel (Table 1), and **32**, whose remarkable activity drop is substantially due to the replacement of 4-DMAP with NBD being unchanged the six-methylene linker. In agreement with the experimental data, we observed a substantial energy gap when comparing the docking scores of **28** (-10.047 kcal/mol) *vs* **32** (-8.121 kcal/mol). Importantly, the value returned by **28** is close to that measured by calibrating the X-ray cognate ligand (-11.08 kcal/mol), thus supporting the robustness of the predicted binding mode. Fig. 13 shows the top-scored docking poses obtained for **28** and **32**. The binding mode observed when inspecting the crystal model of the cognate ligand mostly ruled by hydrophobic interactions is herein fully confirmed. More specifically, the bulky adamantane moiety is accommodated in a hydrophobic subpocket by engaging contacts with F87, F91, F94 and V113 while the dihydroquinolin scaffold establishes T-shaped pi-pi interactions with W258, consistently with the X-ray data of the cognate ligand. As far as the methylene linker and the fluorescent tag are concerned, a different binding mode between the two investigated compounds is observed. More specifically, the fluorescent tag of **28** (4-DMAP) establishes T-shaped pi-pi interactions with both Y190 and F183. In addition, we also detected hydrophobic interactions with I110 residue. A different pose is instead experienced by NBD (**32**), which prefers to look towards L191 and L195 by losing interactions with F183 and Y190. Based on these results, we can here speculate that such a different orientation is probably related to the presence, in NBD, of a nitro substituent making considerably less stable T-shaped pi-pi interactions [80].

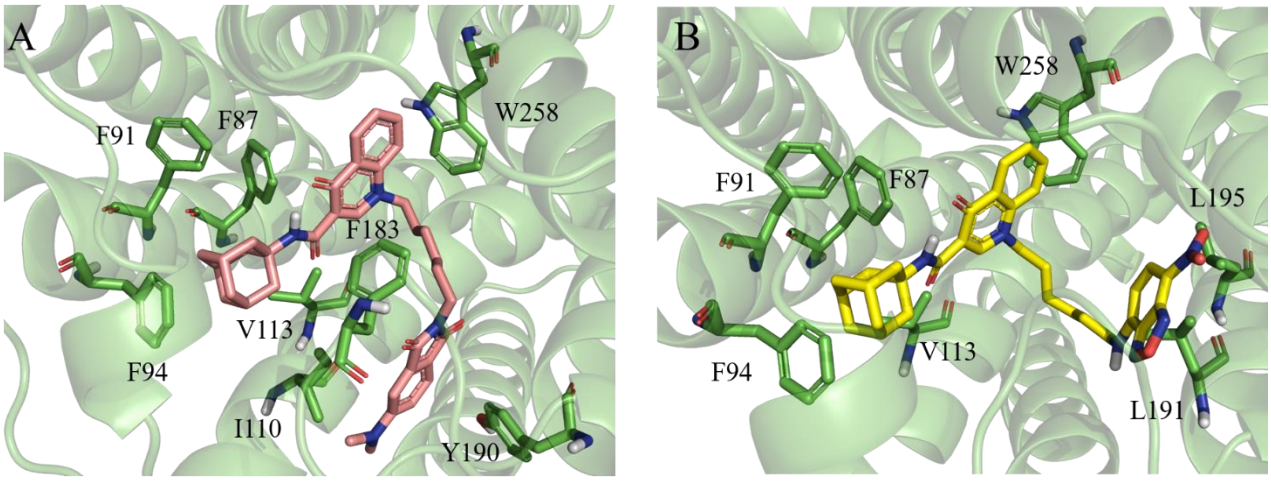

Fig. 13. Top-scored docking poses of compounds **28** (A) and **32** (B) within the binding site of CB2R (PDB code: 5ZTY). For the sake of clarity only polar hydrogen atoms are shown. Important residues are rendered as sticks while protein is represented as cartoon.

4. Conclusions

The design of new fluorescent ligands able to detect CB2R through a specific, green and safe approach, promted us to develop a series of fluorescent compounds based on the *N*-adamantyl-4-oxo-1,4-dihydroquinoline-3-carboxamide scaffold. Different lengths of alkyl chains (from six to twelve methylenes) at the 1-position of such scaffold carrying three different fluorescent tags were explored. Despite a moderate CB2R affinity (K_i = 130 nM), compound **28** bearing a 4-DMAP fluorescent moiety through a hexamethylene linker, emerged as one of the highest affinity CB2R fluorescent ligands known, to the best of our knowledge. Therefore, compound **28**, emerged for the promising compromise between its CBR pharmacodynamic profile (good CB2R affinity and selectivity towards CB1R) and fluorescent properties. Thus, compound **28** ability to detect CB2R by fluorescence studies was investigated by FACS (saturation and competitive binding studies) and fluorescence microscopy (visualization and competitive binding) in diverse cell lines. Either in engineered cells (CB2R-HEK293 cells) or in tumor cells, fluoligand binding assays were successfully conducted, and affinity values comparable to the values by radioligand binding assays were obtained for two reference compounds (GW405833 and WIN55,212-2). Additionally, in these same cells, compound **28** allowed the detection of the presence and quantification of the CB2R, although a strict comparison with the same assay conducted with the radioligand could not be made for the low specific binding obtained with the latter. Moreover, the interactions of compound **28** within the CB2R binding site were deepend by molecular docking simulations, and the comparison with the docking of the NBD-bearing counterpart (i.e. compound **32**) shed light on important features for CB2R high affinity binding. Overall, the results obtained through these studies led to propose compound **28** as a safe and green alternative to the commonly used radioligand based assays, while hints for improving the binding profile and consequently the biological exploitations of this class of compounds are given.

5. Experimental section

5.1 Chemistry

All chemicals, unless otherwise stated, were purchased from Sigma-Aldrich, TCI Chemicals, Alfa Aesar, or Acros Organics. Microwave irradiation was performed in a Biotage Initiator+ with 2−5 mL and 10−20 mL Biotage reaction vials. Thin layer chromatography (TLC) was performed using plates from Merck (silica gel 60 F254). Column chromatography was performed with Merck silica gel 60 Å (63–200 μm) as the stationary phase. Flash chromatographic separations were performed either using Merck silica gel 60 Å (15–40 μm) or on a Biotage SP1 purification system using flash cartridges pre-packed with KP-Sil 60 Å 32–63 μm. Melting points were determined in open capillaries on a Gallenkamp electrothermal apparatus. ^{1}H and ^{13}C NMR spectra were recorded in the indicated solvent on a Varian Mercury-VX spectrometer (300 MHz) or on an Agilent 500-vnmrs500 spectrometer (499.801 MHz). The following data are reported: chemical shift (δ) in ppm, multiplicity (s = singlet, d = doublet, t = triplet, q = quartet, quint = quintet, dd = doublet of doublets, dt = doublet of triplets, m = multiplet, br = broad signal), integration, and coupling constant (*J*) in hertz. ^{13}C NMR (125 MHz) were recorded on a 500-vnmrs500 spectrometer (499.801 MHz) on novel final compounds: chemical shift (δ) in ppm were reported. Recording of mass spectra was done on an HP6890-5973 MSD gas chromatograph/mass spectrometer; only significant m/z peaks, with their percentage of relative intensity in parentheses, are reported. HRMS-ESI analyses were performed on a Bruker Daltonics MicrOTOF-Q II mass spectrometer. All spectra were in accordance with the assigned structures. The purity of target compounds listed in Table 1 was assessed by HPLC. Analytical HPLC analyses were performed on an Agilent 1260 Infinity Binary LC System equipped with a diode array detector using a reversed phase column (Phenomenex Gemini C-18, 5 μm, 250 × 4.6 mm). Isocratic elution was conducted at a flow rate of 1 mL/min with CH_3CN/H_2O (90:10, v/v), unless otherwise stated. UV signal was detected at 254 nm, 280 nm, and 320 nm. All compounds showed > 98% purity.

*5.1.1 General procedure for the synthesis of compounds **8-11** by microwave catalyzed N-alkylation.*

The 4-oxo-1,4-dihydroquinoline core structure **7** (1 g, 4.6 mmol), the appropriate dibromoalkane (13.8 mmol), and K_2CO_3 (1.28 g, 9.3 mmol) were weighted altogether in a 10-20 mL microwave vial and CH_3CN (≈ 12 mL) was added. The vial was sealed, shaken vigorously, and heated in the microwave irradiator at 160 °C for 45 min. After cooling, the solvent was removed by rotary evaporation and the corresponding residue

was partitioned between H_2O (20 mL) and CH_2Cl_2 (20 mL). The aqueous phase was further extracted with CH_2Cl_2 (2 × 20 mL). The combined organic layers were dried over Na_2SO_4 and evaporated under vacuum affording a brownish oil as crude which was purified by chromatography (1:50) with CH_2Cl_2/AcOEt (4:1) as eluent to afford the title compound.

*5.1.1.2 Ethyl 1-(6-bromohexyl)-4-oxo-1,4-dihydroquinoline-3-carboxylate-**8**.*

Compound **7** was alkylated with 1,6-dibromohexane (2.1 mL) to afford **8** as an off-white solid. Yield, 53%; mp: 76-78 °C.

^{1}H-NMR (500 MHz, $CDCl_3$) δ: 1.40 (t, 3H, *J* = 7.1 Hz), 1.40-1.47 (m, 2H), 1.53 (quint, 2H, *J* = 7.5 Hz), 1.87 (quint, 2H, *J* = 7.0 Hz), 1.92 (quint, 2H, *J* = 7.5 Hz), 3.40 (t, 2H, *J* = 7.0 Hz), 4.20 (t, 2H, *J* = 7.5 Hz), 4.41 (q, 2H, *J* = 7.1 Hz), 7.43-7.46 (m, 2H), 7.70 (dt, 1H, J_1 = 7.8 Hz, J_2 = 1.5 Hz), 8.50 (s, 1H), 8.56 (d, 1H, *J* = 7.8 Hz). HRMS-ESI for $C_{18}H_{22}BrNO_3$ (*m*/*z*): $[M+H]^+$ calcd, 380.0856; found, 380.0852; $[M+Na]^+$ calcd, 402.0675; found, 402.0674.

*5.1.1.3 Ethyl 1-(8-bromooctyl)-4-oxo-1,4-dihydroquinoline-3-carboxylate-**9**.* Compound **7** was alkylated with 1,8-dibromooctane (2.5 mL) to afford **9** as an off-white solid. Yield, 55%; mp: 76-80 °C.

^{1}H-NMR (500 MHz, $CDCl_3$) δ: 1.31-1.41 (m, 8H), 1.43 (t, 3H, *J* = 7.1 Hz), 1.81-1.83 (m, 2H), 1.85-1.92 (m, 4H), 3.39 (t, 2H, *J* = 6.8 Hz), 4.17 (t, 2H, *J* = 7.5 Hz), 4.41 (q, 2H , *J* = 7.1 Hz), 7.43-7.45 (m, 2H), 7.68 (dt, 1H, J_1 = 7.8 Hz, J_2 = 1.5 Hz), 8.47 (s, 1H), 8.55 (dd, 1H, J_1 = 8.3 Hz, J_2 = 1.5 Hz). HRMS-ESI for $C_{20}H_{26}BrNO_3$ (*m*/*z*): $[M+H]^+$ calcd, 408.1169; found, 408.1165; $[M+Na]^+$ calcd, 430.0988; found, 430.0988.

*5.1.1.4 Ethyl 1-(10-bromodecyl)-4-oxo-1,4-dihydroquinoline-3-carboxylate-**10**.* Compound **7** was alkylated with 1,10-dibromodecane (3.1 mL) to afford **10** as an off-white solid. Yield, 53%; mp: 73-76 °C.

^{1}H-NMR (500 MHz, $CDCl_3$) δ: 1.29-1.40 (m, 12H), 1.44 (t, 3H, *J* = 7.1 Hz), 1.83 (quint, 2H, *J* = 7.3 Hz), 1.89 (quint, 2H, *J* = 7.3 Hz), 3.40 (t, 2H, *J* = 6.8 Hz), 4.17 (t, 2H, *J* = 7.5 Hz), 4.41 (q, 2H, *J* = 7.1 Hz), 7.43-7.45 (m, 2H), 7.69 (dt, 1H, J_1 = 7.8 Hz, J_2 = 1.5 Hz, aromatic), 8.48 (s, 1H), 8.52 (dd, 1H, J_1 = 7.8 Hz, J_2 = 1.5 Hz, aromatic). HRMS-ESI for $C_{22}H_{30}BrNO_3$ (*m*/*z*): $[M+H]^+$ calcd, 436.1847; found, 436.1847; $[M+Na]^+$ calcd, 458.1307; found, 458.1304.

*5.1.1.5 Ethyl 1-(12-bromododecyl)-4-oxo-1,4-dihydroquinoline-3-carboxylate-**11***. Compound **7** was alkylated with 1,12-dibromododecane (4.53 g) to afford **11** as a brownish oil. Yield, 51%.

^{1}H-NMR (500 MHz, $CDCl_3$) δ: 1.21-1-41 (m, 16H), 1.40 (t, 3H, *J* = 7.1 Hz), 1.81-1.92 (m, 4H), 3.40 (t, 2H, *J* = 7.8 Hz), 4.17 (t, 2H, *J* = 7.5 Hz, 4.40 (q, 2H , *J* = 7.1 Hz), 7.43-7.45 (m, 2H, aromatic), 7.68 (dt, 1H, J_1 = 7.8 Hz, J_2 = 1.5 Hz), 8.48 (s, 1H), 8.55 (dd, 1H, J_1 = 8.3 Hz, J_2 = 1.5 Hz). HRMS-ESI for $C_{24}H_{34}BrNO_3$ (*m*/*z*): $[M+H]^+$ calcd, 464.1795; found, 464.1794; $[M+Na]^+$ calcd, 486.1614; found, 486.1614.

*5.1.2 General procedure for the synthesis of azido derivatives **12-15*.**

A mixture of the appropriate alkylbromide derivative **8-11** (2.37 mmol) and NaN_3 (11.85 mmol, 0.77 g) in dry DMF (10 mL) was stirred at 60 °C for 20 h. The solvent was removed under vacuum. The residue was taken up with H_2O (15 mL) and extracted with CH_2Cl_2 (3 × 10 mL). The combined organic layers were washed with brine (3 × 20 mL), dried over Na_2SO_4 and concentrated under reduced pressure. The resulting crude was purified by column chromatography using CH_2Cl_2/AcOEt (1:1) as eluent to afford the azide derivative.

*5.1.2.1 Ethyl 1-(6-azidohexyl)-4-oxo-1,4-dihydroquinoline-3-carboxylate-**12***. The title compound was obtained as an off-white solid. Yield, 80%; mp, 76-78 °C.

^{1}H-NMR (500 MHz, $CDCl_3$) δ: 1.40-1.46 (m, 7H), 1.59 (quint, 2H, *J* = 6.8 Hz), 1.88-1.94 (m, 2H, *J* = 7.3 Hz), 3.27 (t, 2H, *J* = 6.8 Hz), 4.18 (t, 2H, *J* = 7.3 Hz), 4.40 (q, 2H, *J* = 7.1 Hz), 7.41-7.45 (m, 2H), 7.68 (dt, 1H, J_1 = 7.8 Hz, J_2 = 1.5 Hz), 8.46 (s, 1H), 8.54 (dd, 1H, J_1 = 8.6 Hz, J_2 = 1.5 Hz). HRMS-ESI for $C_{18}H_{22}N_4O_3$ (*m*/*z*): $[M+H]^+$ calcd, 343.1765; found, 343.1767; $[M+Na]^+$ calcd, 365.1584; found, 365.1587.

*5.1.2.2 Ethyl 1-(8-azidooctyl)-4-oxo-1,4-dihydroquinoline-3-carboxylate-**13***. The title compound was obtained as an off-white solid. Yield, 59%; mp: 79-82 °C.

^{1}H-NMR (500 MHz, $CDCl_3$) δ: 1.29-1.40 (m, 8H), 1.43 (t, 3H, *J* = 7.1 Hz), 1.58 (quint, 2H, *J* = 6.8 Hz), 1.89 (quint, 2H, *J* = 7.3 Hz), 3.25 (t, 2H, *J* = 6.8 Hz), 4.17 (t, 2H, *J* = 7.3 Hz), 4.40 (q, 2H , *J* = 7.1 Hz), 7.42-7.45 (m, 2H), 7.68 (dt, 1H, J_1 = 7.8 Hz, J_2 = 1.5 Hz), 8.47 (s, 1H), 8.55 (dd, 1H, J_1 = 7.8 Hz, J_2 = 1.5 Hz). HRMS-ESI for $C_{20}H_{26}N_4O_3$ (*m*/*z*): $[M+H]^+$ calcd, 371.2078; found, 371.2075; $[M+Na]^+$ calcd, 393.1897; found, 393.1894.

*5.1.2.3 Ethyl 1-(10-azidodecyl)-4-oxo-1,4-dihydroquinoline-3-carboxylate-**14**.* The title compound was obtained as a pale-yellow oil. Yield, 91%.

^{1}H-NMR (500 MHz, $CDCl_3$) δ: 1.29-1.40 (m, 20H), 1.43 (t, 3H, *J* = 7.1 Hz), 1.58 (quint, 2H, *J* = 6.8 Hz), 1.89 (quint, 2H, *J* = 7.5 Hz), 3.25 (t, 2H, *J* = 6.8 Hz), 4.17 (t, 2H, *J* = 7.5 Hz), 4.41 (q, 2H , *J* = 7.1 Hz), 7.43-7.45 (m, 2H, *J* = 7.8 Hz), 7.68 (dt, 1H, J_1 = 7.8 Hz, J_2 = 1.5 Hz), 8.48 (s, 1H), 8.56 (dd, 1H, J_1 = 7.8 Hz, J_2 = 1.5 Hz). HRMS-ESI for $C_{22}H_{30}N_4O_3$ (*m*/*z*): $[M+H]^+$ calcd, 399.2391; found, 399.2390; $[M+Na]^+$ calcd, 421.2209; found, 421.2209.

*5.1.2.4 Ethyl 1-(12-azidododecyl)-4-oxo-1,4-dihydroquinoline-3-carboxylate-**15**.* The title compound was obtained as brownish oil. Yield, 90%.

^{1}H-NMR (500 MHz, $CDCl_3$, δ): 1.24-1.39 (m, 16H), 1.43 (t, 7H, *J* = 7.1 Hz), 1.58 (quint, 2H, *J* = 6.8 Hz), 1.88 (quint, 2H, *J* = 7.3 Hz), 3.25 (t, 2H, *J* = 6.8 Hz), 4.17 (t, 2H, *J* = 7.3 Hz), 4.41 (q, 2H , *J* = 7.1 Hz), 7.42-7.45 (m, 2H), 7.66-7.68 (dt, 1H, J_1 = 8.0 Hz, J_2 = 1.5 Hz), 8.48 (s, 1H), 8.55 (dd, 1H, J_1 = 8.0 Hz, J_2 = 1.5 Hz). HRMS-ESI for $C_{24}H_{34}N_4O_3$ (*m*/*z*): $[M+H]^+$ calcd, 427.2704; found, 427.2704; $[M+Na]^+$ calcd, 449.2523; found, 449.2523.

*5.1.3 General procedure for the synthesis of acids **16-19**.*

The appropriate ethyl ester **12-15** (1.90 mmol) was dissolved in a mixture 1:1 of NaOH 2N (15 mL) and EtOH (15 mL) and the reaction mixture was stirred at room temperature for 4 h. The solution was acidified (HCl 2N) and extracted with CH_2Cl_2 (3 × 20 mL). The organic layers were collected, dried over Na_2SO_4, and the solvent was removed by rotary evaporation to give the desired carboxylic acid, which was used without further purification.

*5.1.3.1 1-(6-Azidohexyl)-4-oxo-1,4-dihydroquinoline-3-carboxylic acid-**16**.* The title compound was obtained as a white solid. Yield, 96%; 78-80 °C.

^{1}H-NMR (500 MHz, $CDCl_3$) δ: 1.44-1.47 (m, 4H), 1.58-1.62 (m, 2H), 1.94-1.99 (m, 2H), 3.29 (t, 2H, *J* = 6.8 Hz), 4.33 (t, 2H, *J* = 7.3 Hz), 7.59-7.62 (m, 2H), 7.86 (dt, 1H, J_1 = 7.8 Hz, J_2 = 1.5 Hz), 8.57 (dd, 1H, J_1 = 8.1 Hz, J_2 = 1.5 Hz), 8.76 (s, 1H). COOH proton was not detected. HRMS-ESI for $C_{16}H_{18}N_4O_3$ (m/z):

$[M+H]^+$ calcd, 315.1452; found, 315.1453; $[M+Na]^+$ calcd, 337.1271; found, 337.1271; $[M–H]^–$ calcd 313.1306, found, 313.1307.

*5.1.3.2 1-(8-Azidooctyl)-4-oxo-1,4-dihydroquinoline-3-carboxylic acid-**17**.* The title compound was obtained as an off-white solid. Yield, 93%; mp: 81-84 °C.

^{1}H-NMR (500 MHz, $CDCl_3$) δ: 1.29-1.43 (m, 8H), 1.55-1.62 (m, 2H), 1.94 (quint, 2H, *J* = 7.3 Hz), 3.25 (t, 2H, *J* = 6.8 Hz), 4.32 (t, 2H, *J* = 7.3 Hz), 7.58-7.62 (m, 2H), 7.85 (dt, 1H, J_1 = 7.8 Hz, J_2 = 1.5 Hz), 8.56 (dd, 1H, J_1 = 8.1 Hz, J_2 = 1.5 Hz), 8.75 (s, 1H. COOH proton was not detected. HRMS-ESI for $C_{18}H_{22}N_4O_3$ (m/z): $[M+H]^+$ calcd, 343.1765; found, 343.1763; $[M+Na]^+$ calcd, 365.1584; found, 365.1582; $[M–H]^–$ calcd 341.1619, found, 341.1612.

*5.1.3.3 1-(10-Azidodecyl)-4-oxo-1,4-dihydroquinoline-3-carboxylic acid-**18**.* The title compound was obtained as an off-white solid. Yield, 81%; mp: 83-85 °C.

^{1}H-NMR (500 MHz, $CDCl_3$) δ: 1.29-1.45 (m, 12H), 1.56-1.61 (m, 2H), 1.93 (quint, 2H, *J* = 7.5 Hz), 3.25 (t, 2H, *J* = 6.8 Hz), 4.31 (t, 2H, *J* = 7.5 Hz), 7.58-7.63 (m, 2H), 7.86 (dt, 1H, J_1 = 7.8 Hz, J_2 = 1.5 Hz), 8.57 (dd, 1H, J_1 = 8.1 Hz, J_2 = 1.5 Hz), 8.76 (s, 1H). COOH proton was not detected. HRMS-ESI for $C_{20}H_{26}N_4O_3$ (*m*/*z*): $[M+H]^+$ calcd, 371.2078; found, 371.2075; $[M+Na]^+$ calcd, 393.1897; found, 393.1894; $[M–H]^–$ calcd 369.1932, found, 369.1930.

*5.1.3.4 1-(12-Azidododecyl)-4-oxo-1,4-dihydroquinoline-3-carboxylic acid-**19**.* The title compound was obtained as a brownish sticky solid. Yield, 91%.

^{1}H-NMR (500 MHz, $CDCl_3$): 1.27-1.42 (m, 16H), 1.60 (quint, 2H, *J* = 7.0 Hz), 1.92-1.97 (m, 2H), 3.25 (t, 2H, *J* = 7.0 Hz), 4.31 (t, 2H, *J* = 7.0 Hz), 7.58-7.62 (m, 2H), 7.86 (t, 1H, *J* = 7.3 Hz), 8.57 (d, 1H, *J* = 7.3 Hz), 8.76 (s, 1H). COOH proton was not detected. HRMS-ESI for $C_{22}H_{30}N_4O_3$ (*m*/*z*): $[M+H]^+$ calcd, 399.2391; found, 399.2391; $[M+Na]^+$ calcd, 421.2210; found, 421.2213; $[M–H]^–$ calcd 397.2245, found, 397.2243.

*5.1.4 General procedure for the synthesis of amides **20-23**.*

The appropriate carboxylic acid **16-19** (2.14 mmol) was dissolved in dry DMF (5 mL), DIPEA (6.44 mmol, 1.12 mL) was added at 0° C, and the solution was stirred at 0 °C for 10 min under argon atmosphere. HBTU

(3.21 mmol, 1.22 g) was added to the solution and the reaction mixture was stirred at room temperature for 2 h. 1-Adamantylamine (3.21 mmol, 0.48 g) was added to the solution and the mixture was stirred at room temperature for 18 h under inert atmosphere. The reaction mixture was poured into H_2O (20 mL) and extracted with CH_2Cl_2 (3 × 20 mL). The collected organic layers were washed with HCl 1 N (20 mL), H_2O (20 mL), and brine (3 × 20 mL), dried over Na_2SO_4, and concentrated under vacuum. The crude product was purified by column chromatography using CH_2Cl_2/AcOEt (9:1) as eluent to afford the relative adamantylamide.

*5.1.4.1 N-(Adamantan-1-yl)-1-(6-azidohexyl)-4-oxo-1,4-dihydroquinoline-3-carboxamide-**20**.* The title compound was obtained as an off-white sticky solid. Yield, 83%.

^{1}H-NMR (500 MHz, $CDCl_3$) δ: 1.42-1.45 (m, 4H), 1.57-1.61 (m, 2H), 1.69-1.76 (m, 6H), 1.90-1.93 (m, 2H), 2.08-2.11 (m, 3H), 2.18-2.19 (m, 6H), 3.27 (t, 2H, J = 6.8 Hz), 4.24 (t, 2H, J = 7.3 Hz), 7.47-7.51 (m, 2H), 7.73 (dt, 1H, J_1 = 7.8 Hz, J_2 = 1.5 Hz), 8.54 (dd, 1H, J_1 = 8.3 Hz, J_2 = 1.5 Hz,), 8.74 (s, 1H), 9.93 (s, 1H). HRMS-ESI for $C_{26}H_{33}N_5O_2$ (*m*/*z*): $[M+H]^+$ calcd, 448.2707; found, 448.2708; $[M+Na]^+$ calcd, 470.2526; found, 470.2529.

*5.1.4.2 N-(Adamantan-1-yl)-1-(8-azidooctyl)-4-oxo-1,4-dihydroquinoline-3-carboxamide-**21**.* The title compound was obtained as a brownish solid. Yield, 89%.

^{1}H-NMR (500 MHz, $CDCl_3$) δ: 1.32-1.40 (m, 8H), 1.57 (quint, 2H, J = 6.8 Hz), 1.69-1.76 (m, 6H), 1.88 (quint, 2H, J = 7.3 Hz), 2.08-2.13 (m, 3H), 2.15-2.21 (m, 6H), 3.25 (t, 2H, J = 6.8 Hz), 4.22 (t, 2H, J = 7.3 Hz), 7.46-7.52 (m, 2H), 7.71-7.74 (m, 1H), 8.53 (dd, 1H, J_1 = 8.1 Hz, J_2 = 1.5 Hz), 8.74 (s, 1H), 9.94 (s, 1H). HRMS-ESI for $C_{28}H_{37}N_5O_2$ (*m*/*z*): $[M+H]^+$ calcd, 476.3026; found, 476.3022; $[M+Na]^+$ calcd, 498.2839; found, 498.2840.

*5.1.4.3 N-(Adamantan-1-yl)-1-(10-azidodecyl)-4-oxo-1,4-dihydroquinoline-3-carboxamide-**22**.* The title compound was obtained as a brownish solid. Yield, 77%.

^{1}H-NMR (500 MHz, $CDCl_3$) δ: 1.23-1.42 (m, 12H), 1.58 (quint, 2H, J = 7.1 Hz), 1.69-1.76 (m, 6H), 1.89 (quint, 2H, J = 7.5 Hz), 2.09-2.12 (m, 3H), 2.16-2.19 (m, 6H), 3.25 (t, 2H, J = 7.1 Hz), 4.22 (t, 2H, J = 7.5 Hz), 7.47 (t, 1H, J = 7.6 Hz), 7.51 (d, 1H, J = 8.3 Hz), 7.72 (dt, 1H, J_1 = 7.8 Hz, J_2 = 1.5 Hz), 8.53 (dd, 1H,

J_1 = 7.8 Hz, J_2 = 1.5 Hz), 8.74 (s, 1H), 9.94 (s, 1H). HRMS-ESI for $C_{30}H_{41}N_5O_2$ (*m*/*z*): $[M+H]^+$ calcd, 504.3333; found, 504.3339; $[M+Na]^+$ calcd, 526.3152; found, 526.3157.

*5.1.4.4 N-(Adamantan-1-yl)-1-(12-azidododecyl)-4-oxo-1,4-dihydroquinoline-3-carboxamide-**23***. The title compound was obtained as an off-white sticky solid. Yield, 86%.

^{1}H-NMR (500 MHz, $CDCl_3$) δ: 1.25-1.42 (m, 16H), 1.58 (quint, 2H, *J* = 7.1 Hz), 1.69-1.76 (m, 6H), 1.89 (quint, 2H, *J* = 7.5 Hz), 2.09-2.11 (m, 3H), 2.17-2.19 (m, 6H), 3.25 (t, 2H, *J* = 7.1 Hz), 4.21 (t, 2H, *J* = 7.5 Hz), 7.47 (t, 1H, *J* = 7.6 Hz), 7.51 (d, 1H, *J* = 8.8 Hz), 7.72 (dt, 1H, J_1 = 7.8 Hz, J_2 = 1.5 Hz), 8.53 (dd, 1H, J_1 = 8.1 Hz, J_2 = 1.5 Hz), 8.74 (s, 1H), 9.94 (s, 1H). HRMS-ESI for $C_{32}H_{45}N_5O_2$ (*m*/*z*): $[M+H]^+$ calcd, 532.3646; found, 532.3643; $[M+Na]^+$ calcd, 554.3465; found, 554.3469.

*5.1.5 General procedure for the synthesis of compound **24-27.***

The appropriate azide **20-23** (1.74 mmol) and triphenylphosphine (3.5 mmol, 0.92 g) were dissolved in dry MeOH and stirred at 80 °C for 60 min under inert atmosphere. The solvent was removed under vacuum and the residue was taken up with NaOH 2N (10 mL) and extracted with CH_2Cl_2 (3 × 15 mL). The collected organic layers were washed with brine (3 × 15 mL), dried over Na_2SO_4, and evaporated by rotary evaporation. The resulted crude was purified by column chromatography using CH_2Cl_2/MeOH (gradient 95:5 to 9:1 + 1% Et_3N v/v) as eluent to give the corresponding amine.

*5.1.5.1 N-(Adamantan-1-yl)-1-(6-aminohexyl)-4-oxo-1,4-dihydroquinoline-3-carboxamide-**24***. The title compound was obtained as a white oil. Yield, 83%.

^{1}H-NMR (500 MHz, $CDCl_3$) δ: 1.36-1.47 (m, 6H), 1.68-1.76 (m, 8H), 1.87-1.93 (m, 2H), 2.10-2.12 (m, 3H), 2.17-2.18 (m, 6H), 2.67 (t, 2H, *J* = 6.8 Hz), 4.23 (t, 2H, *J* = 7.3 Hz), 7.47 (t, 1H, *J* = 7.5 Hz), 7.50 (d, 1H, *J* = 8.8 Hz), 7.72 (dt, 1H, J_1 = 8.0 Hz, J_2 = 1.5 Hz), 8.52 (dd, 1H, J_1 = 8.0 Hz, J_2 = 1.5 Hz), 8.74 (s, 1H), 9.94 (s, 1H). HRMS-ESI for $C_{26}H_{35}N_3O_2$ (*m*/*z*): $[M+H]^+$ calcd, 422.2802; found, 422.2807; $[M+Na]^+$ calcd, 444.2621; found, 444.2626.

*5.1.5.2 N-(Adamantan-1-yl)-1-(8-aminooctyl)-4-oxo-1,4-dihydroquinoline-3-carboxamide-**25***. The title compound was obtained as a white solid. Yield, 96%; mp: 90-95 °C.

^{1}H-NMR (500 MHz, $CDCl_3$) δ: 1.29-1.43 (m, 10H), 1.68-1.75 (m, 8H), 1.88 (quint, 2H, *J* = 7.5 Hz), 2.08-2.10 (m, 3H), 2.15-2.21 (m, 6H), 2.66 (t, 2H, *J* = 7.1 Hz), 4.21 (t, 2H, *J* = 7.5 Hz), 7.46 (t, 1H, *J* = 7.6 Hz), 7.50 (d, 1H, *J* = 8.8 Hz), 7.71 (dt, 1H, J_1 = 7.8 Hz, J_2 = 1.5 Hz), 8.52 (d, 1H, *J* = 8.1 Hz), 8.73 (s, 1H), 9.94 (s, 1H). HRMS-ESIfor $C_{28}H_{39}N_3O_2$ (*m*/*z*): $[M+H]^+$ calcd, 450.3115; found, 450.3112; $[M+Na]^+$ calcd, 472.2934; found, 472.2937.

*5.1.5.3 N-(Adamantan-1-yl)-1-(10-aminodecyl)-4-oxo-1,4-dihydroquinoline-3-carboxamide-**26***. The title compound was obtained as a white solid. Yield, 80%; mp: 132-134 °C.

^{1}H-NMR (500 MHz, $CDCl_3$) δ: 1.23-1.46 (m, 14H), 1.69-1.76 (m, 8H), 1.88 (quint, 2H, *J* = 7.5 Hz), 2.09-2.12 (m, 3H), 2.18-2.21 (m, 6H), 2.68 (t, 2H, *J* = 7.1 Hz), 4.22 (t, 2H, *J* = 7.5 Hz), 7.46-7.51 (m, 2H), 7.72 (dt, 1H, J_1 = 7.8 Hz, J_2 = 1.5 Hz), 8.53 (dd, 1H, J_1 = 8.3 Hz, J_2 = 1.5 Hz), 8.74 (s, 1H), 9.95 (s, 1H). HRMS-ESI for $C_{30}H_{43}N_3O_2$ (*m*/*z*): $[M+H]^+$ calcd, 478.3428; found, 478.3429; $[M+Na]^+$ calcd, 500.3247; found, 500.3249.

*5.1.5.4 N-(Adamantan-1-yl)-1-(12-aminododecyl)-4-oxo-1,4-dihydroquinoline-3-carboxamide-**27***. The title compound was obtained as a white solid. Yield, 81%. mp: 135-137 °C.

^{1}H-NMR (500 MHz, $CDCl_3$) δ: 1.25-1.42 (m, 20H), 1.69-1.76 (m, 6H), 1.88 (t, 2H, *J* = 7.5 Hz), 2.09-2.11 (m, 3H), 2.18-2.20 (m, 6H), 2.68 (t, 2H, *J* = 7.1 Hz), 4.22 (t, 2H, *J* = 7.5 Hz), 7.47 (t, 1H, *J* = 7.7 Hz), 7.51 (d, 1H, *J* = 8.8 Hz), 7.72 (dt, 1H, J_1 = 7.7 Hz, J_2 = 1.5 Hz), 8.53 (d, 1H, *J* = 8.3 Hz), 8.74 (s, 1H), 9.95 (s, 1H). HRMS-ESI for $C_{32}H_{47}N_3O_2$ (*m*/*z*): $[M+H]^+$ calcd, 506.3741; found, 506.3745; $[M+Na]^+$ calcd, 528.3566; found, 528.3568.

*5.1.6 General procedure for the synthesis of final compounds **28-31.***

4,4-Dimethylamino phthalic acid (0.87 mmol, 0.182 g) was dissolved in dry DMF (5 mL), DIPEA (5.22 mmol, 0.9 mL) was added at 0° C, and the solution was stirred at 0 °C for 10 min under argon atmosphere. HBTU (2.61 mmol, 0.99 g) was added to the solution and the reaction mixture was stirred at room temperature for 2 h. A solution of the appropriate amine **24-27** (0.7 mmol) in dry DMF (3 mL) was added and the mixture was stirred at room temperature for 18 h under argon atmosphere. The reaction mixture was poured into H_2O (20 mL) and was extracted with CH_2Cl_2 (3 × 20 mL). The collected organic layers were

washed with H_2O (3 × 20 mL) and brine (3 × 20 mL), were dried over Na_2SO_4 and were concentrated under vacuum.

*5.1.6.1 N-(Adamantan-1-yl)-1-(6-(5-(dimethylamino)-1,3-dioxaisoindolin-2-yl)hexyl)-4-oxo-1,4-dihydroquinolin-3-carboxamide-**28**.* The crude product was purified by flash chromatography using CH_2Cl_2/AcOEt (gradient 95:5 to 4:1) as eluent. The resulted solid was recrystallized from CH_2Cl_2/*n*-Hexane to afford **28** as a yellow solid. Yield, 16%.

^{1}H-NMR (500 MHz, $CDCl_3$) δ: 1.37-1.41 (m, 2H), 1.46 (quint, 2H, *J* = 7.6), 1.64-1.76 (m, 8H), 1.88 (m, 2H, *J* = 7.6 Hz), 2.08-2.12 (m, 3H), 2.17-2.18 (m, 6H), 3.11 (s, 6H), 3.62 (t, 2H, *J* = 6.8 Hz), 4.20 (t, 2H, *J* = 7.6 Hz), 6.77 (dd, 1H, J_1 = 8.3 Hz, J_2 = 2.4 Hz), 7.05 (d, 1H, *J* = 2.4 Hz, aromatic), 7.46-7.50 (m, 2H), 7.62 (d, 1H, *J* = 8.3 Hz), 7.70-7.74 (m, 1H), 8.52 (dd, 1H, J_1 = 7.8 Hz, J_2 = 1.5 Hz), 8.72 (s, 1H), 9.92 (s, 1H); ^{13}C NMR (500 MHz, $CDCl_3$) 26.21; 26.27; 28.40; 28.94; 29.54; 36.56;37.28; 40.46; 41.78; 51.63; 54.15; 105.69; 112.91;114.52; 115.78; 117.59; 124.70; 124.83; 127.42; 128.07; 128.20; 129.02; 132.65; 134.71; 138.96; 147.33; 154.31; 163.63, 168.88; 169.27; 176.66. HRMS-ESI for $C_{36}H_{42}N_4O_4$ (*m*/*z*): $[M+H]^+$ calcd, 595.3279; found, 595.3279; $[M+Na]^+$ calcd, 617.3098; found, 617.3099.

*5.1.6.2 N-(Adamantan-1-yl)-1-(8-(5-(dimethylamino)-1,3-dioxaisoindolin-2-yl)octyl)-4-oxo-1,4-dihydroquinolin-3-carboxamide-**29**.* The crude product was purified by flash chromatography using CH_2Cl_2/AcOEt (gradient 95:5 to 4:1) as eluent. The resulted solid was triturated with *n*-Hexane to afford **29** as a yellow solid. Yield, 34%.

^{1}H-NMR (500 MHz, $CDCl_3$) δ: 1.25-1.40 (m, 8H), 1.60-1.66 (m, 2H, *J* = 7.1 Hz), 1.68-1.76 (m, 6H), 1.88 (quint, 2H, *J* = 7.5 Hz), 2.09-2.12 (m, 3H), 2.18-2.19 (m, 6H), 3.10 (s, 6H), 3.61 (t, 2H, *J* = 7.1 Hz), 4.20 (t, 2H, *J* = 7.5 Hz), 6.77 (dd, 1H, J_1 = 8.8 Hz, J_2 = 2.4 Hz), 7.06 (d, 1H, *J* = 2.4 Hz), 7.47 (t, 1H, *J* = 7.8 Hz), 7.51 (d, 1H, *J* = 8.3 Hz), 7.63 (d, 1H, *J* = 8.8 Hz), 7.73 (dt, 1H, J_1 = 7.6 Hz, J_2 = 1.5 Hz), 8.53 (dd, 1H, J_1 = 7.8 Hz, J_2 = 1.5 Hz), 8.73 (s, 1H), 9.94 (s, 1H). ^{13}C NMR (500 MHz, $CDCl_3$) 26.58; 26.62; 28.57; 28.87; 28.96; 29.01; 29.54; 36.56; 37.59; 40.46; 41.79; 105.65; 112.89; 114.47; 115.80; 117.70; 124.64; 124.28; 127.41; 128.07; 128.20; 129.02; 132.63; 134.77; 138.99; 147.36; 154.28; 163.65; 168.93; 169.27; 176.66. HRMS-ESI for $C_{38}H_{46}N_4O_4$ (*m*/*z*): $[M+H]^+$ calcd, 623.3592; found, 623.3595; $[M+Na]^+$ calcd, 645.3411; found, 645.3419.

*5.1.6.3 N-(Adamantan-1-yl)-1-(10-(5-(dimethylamino)-1,3-dioxaisoindolin-2-yl)decyl)-4-oxo-1,4-dihydroquinolin-3-carboxamide-**30**.* The crude product was first purified by column chromatography using CH_2Cl_2/AcOEt (4:1) as eluent. The resulting sample was further purified by flash chromatography through the Biotage SP1 purification system using AcOEt/*n*-Hexane (7:3) as eluent to afford a solid which was recrystallized from ice-cold AcOEt to afford **30** as a yellow solid. Yield, 53%; mp: 132-134 °C.

^{1}H-NMR (500 MHz, $CDCl_3$) δ: 1.24-1.41 (m, 12H), 1.60-1.66 (m, 2H), 1.68-1.76 (m, 6H), 1.87 (quint, 2H, *J* = 7.5 Hz), 2.09-2.12 (m, 3H), 2.18-2.19 (m, 6H), 3.10 (s, 6H), 3.60 (t, 2H, *J* = 7.3 Hz), 4.21 (t, 2H, *J* = 7.5 Hz), 6.77 (dd, 1H, J_1 = 8.3 Hz, J_2 = 2.4 Hz), 7.05 (d, 1H, *J* = 2.4 Hz), 7.46 (t, 1H, *J* = 7.8 Hz), 7.51 (d, 1H, *J* = 8.3 Hz), 7.62 (d, 1H, *J* = 8.3 Hz), 7.72 (dt, 1H, J_1 = 7.8 Hz, J_2 = 1.5 Hz), 8.52 (dd, 1H, J_1 = 7.8 Hz, J_2 = 1.5 Hz), 8.74 (s, 1H), 9.94 (s, 1H). ^{13}C NMR (500 MHz, $CDCl_3$) 26.62; 26.76; 28.65; 29.03; 29.20; 29.25; 29.54; 36.56; 37.72; 40.45; 41.79; 51.64; 54.29; 105.63; 112.87; 114.45; 115.80; 117.75; 124.62; 124.83, 127.42; 128.07; 128.20; 129.02; 132.61; 134.79; 139.00; 147.36, 154.26; 163.67; 168.93; 169.29; 176.66. HRMS-ESI for $C_{40}H_{50}N_4O_4$ (*m*/*z*): $[M+H]^+$ calcd, 651.3905; found, 651.3904; $[M+Na]^+$ calcd, 673.3724; found, 673.3729.

*5.1.6.4 N-(Adamantan-1-yl)-1-(12-(5-(dimethylamino)-1,3-dioxaisoindolin-2-yl)dodecyl)-4-oxo-1,4-dihydroquinolin-3-carboxamide-**31**.* The crude product was purified by flash chromatography starting with CH_2Cl_2 followed by CH_2Cl_2/AcOEt 9:1 as eluent. The resulted solid was recrystallized from ice-cold AcOEt to afford **31** as a yellow solid. Yield, 45%; mp: 123-126 °C.

^{1}H-NMR (500 MHz, $CDCl_3$) δ: 1.23-1.30 (m, 14H), 1.36-1.40 (m, 2H), 1.60-1.76 (m, 8H), 1.87 (quint, 2H, *J* = 7.6 Hz), 2.08-2.12 (m, 3H), 2.16-2.18 (m, 6H), 3.10 (s, 6H), 3.60 (t, 2H, *J* = 7.3 Hz), 4.20 (t, 2H, *J* = 7.6 Hz), 6.76 (dd, 1H, J_1 = 8.3 Hz, J_2 = 2.4 Hz), 7.05 (d, 1H, *J* = 2.4 Hz), 7.46 (t, 1H, *J* = 7.6 Hz), 7.50 (d, 1H, *J* = 8.3 Hz), 7.61 (d, 1H, *J* = 8.3 Hz), 7.71 (dt, 1H, J_1 = 7.8 Hz, J_2 = 1.5 Hz), 8.52 (dd, 1H, J_1 = 8.3 Hz, J_2 = 1.5 Hz), 8.74 (s, 1H), 9.93 (s, 1H). 13C NMR (500 MHz, CDCl3) 26.65; 26.84; 28.72; 29.02; 29.08; 29.17; 29.28; 29.39; 29.41; 29.54; 36.56; 37.77; 40.45; 41.80; 105.62; 112.87; 114.43; 115.79; 117.76; 124.60; 124.81; 127.41; 128.07; 132.59; 134.80; 138.99; 147.36; 154.25; 163.65; 168.93; 169.28; 176.65. HRMS-ESI for $C_{42}H_{54}N_4O_4$ (*m*/*z*): $[M+Na]^+$ calcd, 701.4037; found, 701.4036.

*5.1.7 General procedure for the synthesis of final compounds **32-35**.*

A solution of the appropriate amine **24-27** (0.48 mmol) and 7-chloro-4-nitrobenzoxadiazole (0.96 mmol, 0.157 g) in absolute EtOH (5 mL) was stirred at room temperature for 4 h. The solvent was removed under reduced pressure to provide a crude oil.

*5.1.7.1 N-(Adamantan-1-yl)-1-(6-((7-nitrobenzo[c][1,2,5]oxadiazol-4-yl)amino)hexyl)-4-oxo-1,4-dihydroquinoline-3-carboxamide-**32**.* The crude was purified by flash chromatography using CH_2Cl_2/AcOEt (4:1) and the resulting solid was recrystallized from CH_2Cl_2/*n*-Hexane to give **32** as an orange solid. Yield, 29%.

^{1}H-NMR (500 MHz, $CDCl_3$) δ: 1.42-1.56 (m, 4H), 1.68-1.74 (m, 6H), 1.81 (quint, 2H, *J* = 7.1 Hz), 1.95 (quint, 2H, *J* = 7.1 Hz), 2.08-2.11 (m, 3H), 2.17-2.18 (m, 6H), 3.48-3.52 (m, 2H), 4.28 (t, 2H, *J* = 7.1 Hz), 6.18 (d, 1H, *J* = 8.8 Hz), 6.60 (br s, 1H), 7.48-7.52 (m, 2H), 7.74 (dt, 1H, J_1 = 7.8 Hz, J_2 = 1.5 Hz), 8.48 (d, 1H, *J* = 8.8 Hz), 8.54 (dd, 1H, J_1 = 8.3 Hz, J_2 = 1.5 Hz), 8.75 (s, 1H), 9.94 (s, 1H). ^{13}C NMR (500 MHz, DMSO-d_6) 14.41; 22.51; 25.93; 26.36; 27.98; 28.88; 29.30; 31.40; 36.48; 41.88; 43.93; 50.97; 53.41; 99.66; 111.99; 117.79; 125.33; 126.72; 127.66; 133.33; 138.14; 139.28; 145.85; 148.36; 163.19; 175.90. HRMS-ESI for $C_{32}H_{36}N_6O_5$ (*m*/*z*): $[M–H]^-$ calcd, 583.2674; found, 583.2671.

*5.1.7.2 N-(Adamantan-1-yl)-1-(8-((7-nitrobenzo[c][1,2,5]oxadiazol-4-yl)amino)octyl)-4-oxo-1,4-dihydroquinoline-3-carboxamide-**33**.* The crude product was first purified by flash column chromatography using CH_2Cl_2/AcOEt (gradient 95:5 to 4:1) as eluent. The resulting sample was purified by flash chromatography through the Biotage SP1 purification system using AcOEt/*n*-Hexane (7:3) to provide **33** as an orange solid. Yield, 20%.

^{1}H-NMR (500 MHz, $CDCl_3$) δ: 1.36-1.49 (m, 8H), 1.67-1.73 (m, 6H), 1.79 (quint, 2H, *J* = 7.3 Hz), 1.90-1.95 (m, 2H), 2.07-2.12 (m, 3H), 2.16-2.19 (m, 6H), 3.45-3.55 (m, 2H), 4.26 (t, 2H, *J* = 7.3 Hz), 6.18 (d, 1H, *J* = 8.8 Hz), 6.68 (br s, 1H), 7.48 (t, 1H, *J* = 7.6 Hz), 7.52 (d, 1H, *J* = 8.8 Hz), 7.73 (t, 1H, *J* = 7.6 Hz), 8.49 (d, 1H, *J* = 8.3 Hz), 8.54 (d, 1H, *J* = 7.8 Hz), 8.74 (s, 1H), 10.00 (s, 1H). ^{13}C NMR (500 MHz, $CDCl_3$) 26.08; 26.64; 28.32; 28.58; 28.62; 28.78; 29.50; 36.50; 41.82; 43.83; 51.72; 53.84; 98.47; 112.73; 115.77; 124.96; 127.51; 128.11; 128.21; 129.02; 132.67; 136.47; 138.91; 143.96; 144.28; 147.46; 163.69; 176.70. HRMS-ESI for $C_{34}H_{40}N_6O_5$ (*m*/*z*): $[M+H]^+$ calcd, 613.3133; found, 613.3130; $[M+Na]^+$ calcd, 635.2952; found, 635.2950; $[M–H]^-$ calcd, 611.2982; found, 611.2980.

*5.1.7.3 N-(Adamantan-1-yl)-1-(8-((7-nitrobenzo[c][1,2,5]oxadiazol-4-yl)amino)decyl)-4-oxo-1,4-dihydroquinoline-3-carboxamide-**34**.* The crude was purified by flash chromatography using CH_2Cl_2/AcOEt (gradient 95:5 to 4:1) as eluent to give **34** as an orange solid. Yield, 34%.

^{1}H-NMR (500 MHz, $CDCl_3$) δ: 1.24-1.40 (m, 8H), 1.45 (m, 2H, *J* = 7.6 Hz), 1.54-1.58 (m, 2H), 1.69-1.75 (m, 6H), 1.79 (quint, 2H, *J* = 7.3 Hz), 1.90 (quint, 2H, *J* = 7.3 Hz), 2.09-2.11 (m, 3H), 2.18-2.19 (m, 6H), 3.48-3.52 (m, 2H), 4.26 (t, 2H, *J* = 7.3 Hz), 6.18 (d, 1H, *J* = 8.8 Hz), 6.43 (br s, 1H), 7.48 (t, 1H, *J* = 7.6 Hz), 7.51 (d, 1H, *J* = 8.8 Hz), 7.72 (dt, 1H, J_1 = 7.8 Hz, J_2 = 1.5 Hz), 8.49 (d, 1H, *J* = 8.8 Hz), 8.54 (dd, 1H, J_1 = 8.3 Hz, J_2 = 1.5 Hz), 8.76 (s, 1H), 9.96 (s, 1H). ^{13}C NMR (500 MHz, $CDCl_3$) 22.68; 25.72; 26.46; 26.80; 28.46; 28.79; 28.88; 29.01; 29.09; 29.42; 29.52; 29.68; 31.89; 32.80; 36.54; 41.81; 43.79; 51.68; 54.16; 98.46; 112.83; 115.77; 124.89; 125.27; 127.48; 128.099; 128.20; 129.02; 132.63; 136.45; 138.97; 143.92; 144.28; 147.41; 163.67; 176.68. HRMS-ESI for $C_{36}H_{44}N_6O_5$ (*m*/*z*): $[M+Na]^+$ calcd, 663.3265; found, 663.3267; $[M–H]^–$ calcd, 639.3295; found, 639.3290.

*5.1.7.4 N-(Adamantan-1-yl)-1-(8-((7-nitrobenzo[c][1,2,5]oxadiazol-4-yl)amino)dodecyl)-4-oxo-1,4-dihydroquinoline-3-carboxamide-**35**.* The crude product was first purified by flash column chromatography using CH_2Cl_2/AcOEt (gradient 95:5 to 9:1) as eluent. The resulting sample was further purified by flash column chromatography (1:30) using *n*-Hexane/AcOEt (gradient 7:3 to 3:7) to provide **35** as a red oil. Yield, 32%.

^{1}H-NMR (500 MHz, $CDCl_3$) δ: 1.24-1.40 (m, 14H), 1.47 (quint, 2H, *J* = 7.5 Hz), 1.68-1.75 (m, 6H), 1.80 (quint, 2H, *J* = 7.3 Hz), 1.88 (quint, 2H, *J* = 7.3), 2.08-2.12 (m, 3H), 2.17-2.18 (m, 6H), 3.48-3.51 (m, 2H), 4.22 (t, 2H, *J* = 7.3 Hz), 6.16 (d, 1H, *J* = 8.3 Hz), 6.44 (br s, 1H), 7.46 (t, 1H, *J* = 7.6 Hz), 7.51 (d, 1H, *J* = 8.8 Hz), 7.71 (dt, 1H, J_1 = 7.8 Hz, J_2 = 1.5 Hz), 8.48 (d, 1H, *J* = 8.3 Hz), 8.52 (dd, 1H, J_1 = 7.8 Hz, J_2 = 1.5 Hz), 8.75 (s, 1H), 9.95 (s, 1H). ^{13}C NMR (500 MHz, $CDCl_3$) 26.54; 26.87; 28.49; 28.90; 29.09; 29.19; 29.27; 29.29; 29.39; 28.53; 29.64; 29.67; 36.55; 41.81; 43.99; 51.66; 54.24; 98.47; 112.82; 115.79; 124.86; 127.43; 128.07; 132.62; 136.49; 138.97; 143.91; 144.26; 147.39; 163.68; 176.66. HRMS-ESI for $C_{38}H_{48}N_6O_5$ (*m*/*z*): $[M+Na]^+$ calcd, 691.3578; found, 691.3579; $[M–H]^–$ calcd, 667.3613; found, 667.3614.

*5.1.8 General procedure for the synthesis of compounds **36** and **37** by nucleophilic addition to FITC.* Fluorescein isothiocyanate (0.76 mmol, 0.29 g) was dissolved in dry DMF (2 mL), and DIPEA (0.05 mmol,

0.06 g) and a solution of the appropriate amine **24 or 26** (0.63 mmol) in dry DMF (3 mL) were added in a dropwise manner. The mixture was stirred at room temperature for 1 h. The reaction mixture was poured into H_2O (10 mL) and was extracted with CH_2Cl_2 (6 × 10 mL). The collected organic layers were washed with H_2O (1 × 20 mL) and brine (2 × 20 mL), dried over Na_2SO_4 and concentrated under vacuum to afford a crude oil.

*5.1.8.1 N-(adamantan-1-yl)-1-(6-(3-(3',6'-dihydroxy-3-oxo-3H-spiro[isobenzofuran-1,9'-xanthen]-5-yl)thioureido)hexyl)-4-oxo-1,4-dihydroquinoline-3-carboxamide-**36***. The crude mixture was purified by column chromatography using AcOEt as eluent. The resulting sample was further purified by column chromatography using CH_2Cl_2/MeOH (95:5) to provide the title compound as a yellow oil. Yield, 18%.

^{1}H-NMR (500 MHz, Acetone-d_6) δ: 1.30-1.76 (m, 12H), 1.85-2.00 (m, 2H), 2.10-2.20 (m, 9H), 3.55-3.65 (m, 2H), 4.51-4.56 (m, 2H), 6.55-6.72 (m, 6H), 7.14 (d, 1H, J = 8.3 Hz), 7.52 (t, 1H, J = 8.0 Hz), 7.80 (br s, 1H), 7.82-7.85 (m, 1H), 7.88-7.95 (m, 2H), 8.28 (s, 1H), 8.43 (dd, 1H, J_1 = 7.7 Hz, J_2 = 1.5 Hz), 8.80 (s, 1H), 9.05 (br s, 2H), 9.70 (br s, 1H), 10.20 (br s, 1H). HRMS-ESI for $C_{47}H_{46}N_4O_7S$ (*m*/*z*): $[M+Na-2H]^-$ calcd, 831.2828; found, 831.2829.

*5.1.8.2 N-(adamantan-1-yl)-1-(10-(3-(3',6'-dihydroxy-3-oxo-3H-spiro[isobenzofuran-1,9'-xanthen]-5-yl)thioureido)decyl)-4-oxo-1,4-dihydroquinoline-3-carboxamide-**37***. The crude mixture was purified by column chromatography using AcOEt as eluent. The resulting sample was further purified by column chromatography using CH_2Cl_2/MeOH (95:5) to provide the title compound as a yellow oil. Yield, 12%.

^{1}H-NMR (500 MHz, Acetone-d_6) δ: 1.20-1.90 (m, 22H), 2.00-2.20 (m, 9H), 3.60-3.65 (m, 2H), 4.53-4.58 (m, 2H), 6.52-6.72 (m, 6H), 7.11 (d, 1H, J = 8.1 Hz), 7.54 (t, 1H, J = 8.1 Hz), 7.81-7.95 (m, 2H), 8.15-8.20 (m, 2H), 8.28 (s, 1H), 8.46 (dd, 1H, J_1 = 7.7 Hz, J_2 = 1.5 Hz), 8.85 (s, 1H), 9.15 (br s, 2H), 9.80 (br s, 1H), 10.00 (br s, 1H). HRMS-ESI for $C_{51}H_{54}N_4O_7S$ (*m*/*z*): $[M+Na-2H]^-$ calcd, 887.3454; found, 887.3451.

5.2 Biology

5.2.1 Materials

Cell culture reagents were purchased from Celbio s.r.l. (Milano, Italy). CulturePlate 96/wells plates were purchased from PerkinElmer Life Science; GW405833 and (R)-(+)-WIN 55,212-2 were obtained from

TOCRIS (Milan, Italy); Multiscreen HTS filter plates were purchased by Merck Millipore (Ireland). OptiPhase Supermix and [3H] -CP55940 were purchased from PerkinElmer Life Science.

5.2.2 CNR2 clone amplification

A vector containing the coding sequence of the human CNR2 gene (CNR2-pcDNA3.1, Clone ID: OHu29190D) was purchased from GenScript (Piscataway, NJ, USA) and a chemically competent E. coli TOP10 strain (PA1-850, Thermo Fisher Scientific, San Jose, CA, USA) was used for plasmid propagation. DNA plasmids were then purified using GenElute™ HP Endotoxin-Free Plasmid Maxiprep Kit (Sigma–Aldrich, St Louis, MO, USA) following the manufacturer's instructions. Briefly, an overnight recombinant TOP10 culture was harvested by centrifugation and subjected to alkaline-SDS lysis. A binding solution was added after lysate clarification by filtration. The plasmid DNA was captured on silica, washed twice to remove contaminants and eluted in endotoxin-free water. The recovered plasmid DNA was detected in agarose gel by using Green Gel Plus (Fisher Molecular Biology,Trevose, PA, USA).

5.2.3 Stable transfection of HEK293 cells

Cells were seeded in six-well plates. Stable transfection experiments were performed when cells were about 70–80% confluent by using CNR2-pcDNA3.1 and FugeneHD (Promega, Madison, WI, USA) according to the manufacturer's protocol. Twenty four to forty eight hours after transfection the cells were subjected to drug selection at 1 mg/ml G-418 (Sigma–Aldrich) to determine stable transfection. Antibiotic-resistant colonies that appeared after 2–3 weeks were expanded in new dishes under selection. In some experiments, the cells were further expanded without antibiotic selection.

The cells were tested by western blot analysis and radioligand binding assay identifying the clones overexpressing the CB2R.

5.2.4 Cell cultures

CB2R-HEK293- and CB1R-HEK293 cells were grown in DMEM high glucose supplemented with 10% fetal bovine serum, 2 mM glutamine, 100 U/mL penicillin, 100 μg/mL streptomycin, 0.1 mg/mL G418, in a humidified incubator at 37 °C with a 5 % CO_2 atmosphere.

MCF7 were cultured in DMEM high glucose, U87-MG in DMEM, U-2OS in IDMDM, PANC1, PC3 and HT29 cells in were grown in RPMI-1640 supplemented with 10% fetal bovine serum (FBS), 2 mM

glutamine, 100 U/mL penicillin, 100 μg/mL streptomycin, MCF7/DX and HT29/DXcells were grown in the indicated medium containing 40 nM and 100 nM doxorubicin, respectively, to mantain the chemoresistant phenotype.

5.2.5 Radioligand binding assay

5.2.5.1 Membrane preparations for CB1 and CB2 receptors assays

Membranes of HEK293 cells recombinantly expressing the human CB1 receptor subtype, were prepared by scratching the cells off the previously frozen cell culture dishes in Phosphate Buffered Saline (PBS, pH 7.4). The cell suspension was centrifuged at 800 × g for 15 min and the pellet was resuspended and homogenized on ice for 1 min using a dounce homogenizer, and subsequently spun down for 5 min at 4 °C and 500g. The supernatant was centrifuged for 20 min at 25,000g. The obtained membrane pellets were resuspended in buffer A (10 mM $NaHCO_3$, 10 mM EGTA, 10 mM EDTA, 1 × protease inhibitors cocktail (Sigma Aldrich), pH=7.4) and centrifuged for 20 min at 25,000g. The pellet was resuspended in the required amount of 25 mM Tris-HCl puffer, 5 mM $MgCl_2$, 1mM EDTA, pH 7.4. Aliquots of the membrane preparation were stored at -80 °C until being used.

Membranes of HEK293 cells recombinantly expressing the human CB2 receptor subtypes and of the selected cancer cell lines (MCF7, MCF7-DX, HT29, HT29-DX, PANC1 and PC3) were prepared by scratching the cells off the previously frozen cell culture dishes in ice-cold hypotonic buffer (5 mM Tris-HCl, 2 mM EDTA, pH 7.4). The cell suspension was homogenized on ice for 1 min using an Ultra-Turrax (T25basic, IKALABORTECHNIK, Higashiosaka, Japan) followed by further homogenization for 1 min with a dounce homogenizer, and subsequently spun down for 10 min at 4 °C and 1000g. The supernatant was centrifuged for 60 min at 48,000g. The obtained membrane pellets were resuspended and homogenized in the required amount of 50 mM Tris-HCl puffer, pH 7.4. Aliquots of the membrane preparation were stored at -80 °C until being used [81].

5.2.5.2 Radioligand competition binding assays at CB2 receptors

Competition binding assays were performed using the CB agonist radioligand [3H](-)-cis-3-[2-hydroxy-4-(1,1-dimethylheptyl)phenyl]-trans-4-(3-hydroxypropyl)cyclohexanol (CP55,940), PerkinElmer Italia SPA, Milano, Italy) and the membrane preparations of the HEK293 cells stably expressing CB receptor subtype 2

(100µg protein/well) as source for human CB2 receptor. After addition of 25µL of the test compounds at different concentrations (10 µM-100 nM), 25µL of [3H]CP55,940 solution in assay buffer (at final concentration of 0.2 nM), and 100 µL of membrane preparation to 100 µL of assay buffer (50 mM Tris, 2,5 mM EGTA, 5 mM $MgCl_2$, 0.1 % fatty acid fere bovine serum albumine BSA, pH 7.4), the suspension was incubated for 90 minutes at 30°C. Total binding was determined without the test compounds. Nonspecific binding was determined in the presence of 10 µM GW405833. Incubation was terminated by rapid filtration through a GF/C glass fibre filter (Merck Millipore, Ireland) presoaked for 30 minutes with 0.05 % aq. Polyethyleneimine solution, using a 96-channel cell harvester (Merck Millipore, Ireland). The filter was washed three times with 100 µL ice-cold washing buffer (50 mM Tris, 2,5 mM EGTA, 5 mM $MgCl_2$, 1 % BSA, pH 7.4),) and then dried for 1.5 h at 50 °C. Radioactivity on the filter was determined in a MicroBeta JET counter (Perkin- Elmer, Boston, MA, USA) after 6 h of preincubation with 100 µl of scintillation cocktail (OptiPhase superMix, Perkin- Elmer). Data were obtained in three independent experiments, performed in triplicates. Data were analyzed using GraphPad Prism Version 7 (San Diego, CA, USA). For the calculation of K_i values, the Cheng-Prusoff equation and a Kd value of 1.5 nM ([^{3}H]CP55,940 at CB2) were used.

5.2.5.3 Radioligand competition binding assays at CB1 receptors

Cannabinoid CB1 receptor competition binding experiments were carried out in a polypropilene 96-well plate. In each well was incubated 20 µg of membranes from HEK 293-hCB1 cell line and prepared in our laboratory (Lot: A010/15-05-12, protein concentration=2750 µg/ml), 0.8 nM [^{3}H]-CP55940 (164.9 Ci/mmol, 1 mCi/ml, Perkin Elmer NET1051250UC) and compounds studied and standard. Non-specific binding was determined in the presence of Surinabant 10 µM. The reaction mixture was incubated at 30°C for 60 min, 200 µL was trasnfered to GF/C 96-well plate (Millipore, Madrid, Spain) pretreated with binding buffer (Tris-HCl 50 mM, EDTA 1 mM, MgCl2 5 mM, BSA 0.5%, pH=7.4), after was filtered and washed four times with 250 µl wash buffer (Tris-HCl 50 mM, EDTA 1 mM, $MgCl_2$ 5 mM, BSA 0.5%, pH=7.4), before measuring in a microplate beta scintillation counter (Microbeta Trilux, PerkinElmer, Madrid, Spain). Data were obtained in three independent experiments, performed in triplicates.

5.2.5.4 Saturation binding assay at CB2 receptors with radioligand.

Saturation binding assays were performed using different concentrations (0.001-1 nM) of the CB agonist radioligand [^{3}H](-)-cis-3-[2-hydroxy-4-(1,1-dimethylheptyl)phenyl]-trans-4-(3-hydroxypropyl)cyclohexanol (CP55,940), PerkinElmer Italia SPA, Milano, Italy) and the membrane preparations of the selected cancer cell lines (MCF7, MCF7-DX, HT29, HT29-DX, PANC1, PC3 and CB2R-HEK293) (100 μg protein/well) as source for human CB2 receptor. After addition of 50 μL of [^{3}H]CP55,940 solution in assay buffer at different concentrations (0.01-7 nM for CB2R-HEK293 or 0.01-1 nM for all of the other cell lines) and 100 μL of membrane preparation to 300 μL of assay buffer (50 mM Tris, 2.5 mM EGTA, 5 mM $MgCl_2$, 0.1 % fatty acid fere bovine serum albumine BSA, pH 7.4), the suspension was incubated for 90 minutes at 30°C. The incubation was stopped by rapid filtration on Whatman GF/C glass microfiber filters (pre-soaked in 0.05% aq. polyethyleneimine solution, for 30 min). The filters were washed with 3 × 1 mL of ice-cold washing buffer (50 mM Tris, 2,5 mM EGTA, 5 mM MgCl2, 1 % BSA, pH 7.4). Total binding was determined without the cold compound GW405833 while the nonspecific binding was determined in the presence of 10 μM GW405833. Radioactivity on the filter was determined in a TRI CARB 2810TR scintillation counter (PerkinElmer Italia SPA, Milano, Italy). Data were obtained in three independent experiments, performed in triplicates. Data were analyzed using GraphPad Prism Version 7 (San Diego, CA, USA).

5.2.3 Fluorescence spectroscopy

Emission spectra of all target compound were determined in $CHCl_3$, DMSO, EtOH, and PBS. In all experiments, the excitation and the emission bandpass was set at 5 nm. The emission spectra were obtained from 300 to 800 nm, with excitation set at the appropriate excitation wavelength. The excitation spectra were obtained from 200 to 800 nm. Absorption spectra were recorded with a Shimadzu UV-1800 spectrophotometer, and fluorescence spectra were obtained with a Tecan Infinite M1000 Pro spectrofluorometer.

5.2.4 Cell antiproliferative effect

The antiproliferative effect of **28** on all the selected cells was evaluated through the 3-[4,5-dimethylthiazol-2-yl]-2,5-diphenyltetrazoliumbromide (MTT) assay as reported by Colabufo et al. [82] with minor modifications. The studied cells were seeded into 96-well plates in the absence and presence of known concentrations of **28** for 24h. In each well 10 μl of MTT solution (5 mg/ml) freshly prepared was added and

the platewas incubated in a humidified atmosphere 5% CO2 at 37 °C for 3–4 h. MTT solution was removed and 100 µl of EtOH/DMSO (1:1) was added to each well to dissolve the blue formazan solid crystals. The optical density was measured at 570 nm and 650 nm wavelengths using Victor3, from PerkinElmer Life Sciences. Data were obtained in three independent experiments, performed in triplicates.

5.2.5 Flow cytometry analysis

Three experimental sets were performed:

1) 1 x 10^5 cells were seeded and incubated for 90 minutes with increasing concentrations (0 nM-100 nM, 1 µM, 10 µM) of the CB2R-fluorescent ligand **28** alone (dose-dependence experiments);

2) 1 x 10^5 cells were seeded and incubated for 90 minutes with increasing concentrations (0 nM-0.01 nM, 0.1 nM, 1 nM, 10 nM, 100 nM, 1 µM, 10 µM) of WIN 55,212-2/GW405833 co-incubated with 10 µM **28** (competition binding assays);

3) 1 x 10^5 cells were seed and incubated for 90 minutes with increasing concentrations (0 nM -0.1 nM, 1 nM, 10 nM, 100 nM, 1 µM, 10 µM) of **28** co-incubated with 10 µM GW405833 (saturation binding assays).

Cells were then washed, detached with Cell Dissociation solution (Sigma Chemicals. Co), centrifuged at 12,000 g for 5 minutes and re-suspended in 0.5 mL PBS. The fluorescence was read using a EasyCyte Guava glow cytometer (Millipore), using λ excitation = 420 nM, λ emission = 520 nM, and analyzed with the Incyte software (Millipore). The results were expressed as relative fluorescence units (RFU) of the mean fluorescence intensity (MFI). Data were obtained in three independent experiments, performed in triplicates.

5.2.6 B_{max} calculation and immunoprecipitation

1 x 10^{10} HEK293 cells overexpressing CB2R were incubated with increasing concentrations of the fluoligand **28** (ranging from 0.01 nM to 10 µM) in the absence and in the presence of a fixed dose of the CB2R "cold" reference compound GW405833 10µM. 1 x 10^5 cells were used in flow cytometry assays to calculate the RFU. 1 x 10^5 cells subjected to the biotinylation assays to isolate the plasma-membrane associated proteins, as reported previously [83]. Plasma-associated proteins were quantified by the BCA kit (Sigma Chemicals Co.), as per manufacturer's instruction. 100 µg proteins were immuno-precipitated overnight at 4°C using an anti-CB2R antibody (Santa Cruz Biotechnology Inc.) and 25 µl of PureProteome protein A and protein G

Magnetic Beads (Millipore). The amount of immunopreciptated CB2R was quantified using the BCA kit. The absorbance of samples containing the anti-CB2R antibody immunoprecipitated in the same experimental conditions without cells was used as a blank and was subtracted from the absorbance of each samples, to assess the amount of CB2R. This amount, expressed as mg proteins, was correlated with the RFU obtained by flow cytometry. Data were obtained in two independent experiments, performed in triplicates.

5.3 Statistical analysis

All data in the text and figures are provided as means ± SEM. The results were analysed by a Student's t-test and ANOVA test, using Graph-Pad Prism (Graph-Pad software, San Diego, CA, USA). $p < 0.05$ was considered significant.

5.4 Immunofluorescence Studies

5.4.1 Immunofluorescence labeling of CB2R

CB2R-HEK-293 and HEK-293 wild type were seeded at a density of 50,000 cells per well in 96 well Collagen I-coated CellCarrier™ plate (PerkinElmer) and incubated for 18 h at 37 °C and 5% CO_2. Cells were fixed with paraformaldehyde (PFA) 4% for 30 mins at r.t.. After two PBS washes cells were permeabilized with Triton X-100 0.1% for 10 min at r.t. After two PBS washes, fixed cells were incubated with blocking buffer composed by 1% BSA, 22.52 mg/mL glycine in PBST (PBS + 0.1% Tween 20) for 30 minutes at r.t.. Glycine was added to block non-specific antibody binding since fixation was performed with PFA. Cells were then incubated 1 h at r.t. with an anti-CB2R mouse monoclonal antibody (dilution 1:100; CB2(3C7):sc-293188, Santa Cruz Biotechnology, Inc.) or with 1% BSA in PBST (non-immune control). After three rinses with PBS, cells were incubated with fluorescent donkey anti-mouse IgG antibody [dilution 1:500; Donkey anti-Mouse IgG (H + L) Secondary Antibody, Alexa Fluor™ 594 conjugate, Thermo-Fisher Scientific] for1 h at r.t. in darkness. Thereafter, cells were rinsed three times and stained with DAPI (dilution: 1 mg/mL) for 10 min at r.t. in darkness. Finally, after PBS washes, PBS (100 mL) were dispensed and the plate was tightly sealed with sealing foil. The plate was then imaged by the PerkinElmer Operetta® High Content Screening system using the 20 long WD objective.

*5.4.2 High Content imaging of CB2R-HEK-293 with **28***

HEK-293 CB2R were seeded at a density of 50,000 cells per well in 96 well Collagen I-coated CellCarrier™ plate (PerkinElmer) and incubated for 18 h at 37 °C and 5% CO_2. Cells were fixed with paraformaldehyde (PFA) 4% for 30 mins at r.t.. After two PBS washes cells were incubated with 22.52 mg/mL glycine in PBS for 30 minutes at r.t.. After one rinse with PBS, cells were incubated 90 mins at r.t. in darkness with **28** (0.1-50μM). After two PBS washes cells were stained with Syto™85 (S11366, Invitrogen) orange fluorescent nucleic acid stain 2 μM for 10 min at r.t. in darkness. Finally, after PBS washes, PBS (100 mL) were dispensed and the plate was tightly sealed with sealing foil. The plate was then imaged by the PerkinElmer Operetta® High Content Screening system using the 20 long WD objective.

5.4.3 High Content imaging of competition binding assay with GW405833

CB2R-HEK-293 were seeded at a density of 50,000 cells per well in 96 well Collagen I-coated CellCarrier™ plate (PerkinElmer) and incubated for 18 h at 37 °C and 5% CO_2. Cells were fixed with paraformaldehyde (PFA) 4% for 30 mins at r.t. After two PBS washes cells were incubated with 22.52 mg/mL glycine in PBS for 30 minutes at r.t.. After one rinse with PBS, cells were co-incubated 90 mins at r.t. in darkness with a fixed concentration of **28** (15μM) and increasing GW405833 concentrations (0.01 nM-10 μM). After two PBS washes cells were stained with Syto™85 (S11366, Invitrogen) orange fluorescent nucleic acid stain 2 μM for 10 min at r.t. in darkness. Finally, after PBS washes, PBS (100 mL) were dispensed and the plate was tightly sealed with sealing foil. The plate was then imaged by the PerkinElmer Operetta® High Content Screening system using the 20 long WD objective.

For all high content imaging analysis, the sequence “RMS Cytoplasmic Marker” from the Harmony database was used to quantify fluorescence intensity. The channels used were fixed at λ_{ex}= 420nm λ_{em}=520nm for SM15, λ_{ex}= 590nm λ_{em}=640nm for CB2R, λ_{ex}= 567nm λ_{em}=583nm for Syto85, λ_{ex}= 410nm λ_{em}=530nm the for DAPI.

5.5 Molecular docking simulations

Compounds **28** and **32** were docked on the recently published crystal structure of CB2 (PDB code: 5ZTY, 79). The retrieved .pdb file was prepared using Protein Preparation Wizard Schrödinger Suite 2018-4 [84] for adding missing hydrogen atoms, reconstructing incomplete side chains and assigning favorable protonation states at physiological pH. In order to generate all the possible tautomers and ionization states at a pH value of 7.0 ± 2.0, the ligands were prepared using LigPrep [85]. The obtained files were used for docking simulations performed by Grid-based ligand docking with energetics (GLIDE) [84, 86]. During the docking process, full flexibility was allowed for the ligands while the protein was held fixed. The default Force Field OPLS_2005 [87] and the standard precision (SP) protocol were employed. In particular, in order to properly explore the conformational space of the ligands during the performed simulations, we increased the number of poses per ligand generated in the initial phase of docking from 5000 (default setting) to 500000 and the number of poses per ligand kept for energy minimization from 400 (default setting) to 2000. A cubic grid centered on the cognate ligand (i. e. N-(adamantan-1-yl)-1-(5-hydroxypentyl)-4-methyl-5-phenyl-1H-pyrazole-3-carboxamide) and having an edge of 15 Å for the inner box and 31 Å for the outer box was used. Such a protocol was tested by redocking the cognate ligand into its corresponding binding site. In particular, it moved back to the original positions with a root mean square deviation (RMSD) equal to 0.4 Å (value computed taking into account all the heavy atoms) thus supporting the robustness of the employed docking procedure. Since the cognate ligand shares a common substructure with both **28** and **32**, docking simulations of both the ligands were performed restricting the explored conformational space so that only poses matching the crystallographic coordinates of such substructure (tolerance equal to 1.5 Å) were generated. 3D PDB files for Fig. 13 are reported in the supporting information.

ASSOCIATED CONTENT

* Supporting Information

In vitro radioligand saturation binding assay in CB2R-HEK293 cells (Figure S1).

Flow cytometry analysis in CB2R-HEK293 (Figure S2).

Cytotoxicity of compound **28**: (Table S1)

Author Information

Corresponding Authors

*E-mail: marialessandra.contino@uniba.it

Phone: +39-0805442747

*E-mail: carmen.abate@uniba.it

Phone: +39-0805442231

Author Contributions

The manuscript was written through contributions of all authors. All authors have given approval to the final version of the manuscript.

#F.S. and R.G. contributed equally.

Notes

The authors declare no competing financial interest.

Acknowledgments

C. R. thanks the Italian Cancer Research Association AIRC (IG21408) for financial support.

Abbreviations Used

GPCR, G-protein-coupled receptor; ECS, EndoCannabinoid System; CB2R, Cannabinoid receptor subtype 2; CB1R, cannabinoid receptor subtype 1; CNS, Central Nervous System; PET, Positron Emission Tomography; MRI, Magnetic Resonance Imaging; NBD, 7-nitrobenzoxadiazole NIR, Near-InfraRed; 4-DMAP, 4-dimethylaminophthalimide; FTU, Fluorescein-thiourea FITC, Fluorescein isothiocyanate; FACS, Fluorescence-activated cell sorting.

References

[1] S. Pisanti, P. Picardi, A. D'Alessandro, C. Laezza, M. Bifulco, The endocannabinoid signaling system in cancer, Trends Pharmacol Sci. 34 (2013) 273–282.

[2] F. Spinelli, E. Capparelli, C. Abate, N.A. Colabufo, M. Contino, Perspectives of Cannabinoid Type 2 Receptor (CB2R) Ligands in Neurodegenerative Disorders: Structure-Affinity Relationship (SAfiR) and Structure-Activity Relationship (SAR) Studies. J. Med. Chem. 60 (2017) 9913–9931.

[3] M. Guzmán, Cannabinoids: potential anticancer agents. Nat Rev Cancer. 3 (2003), 745–755.

[4] D. Piomelli, The molecular logic of endocannabinoid signalling. Nat. Rev. Neurosci. 4 (2003), 873–884.

[5] A. C. Howlett, Cannabinoid receptor signaling. Handb. Exp. Pharmacol. 168 (2005) 53–79.

[6] E. Moreno, M. Cavic, A. Krivokuca, V Casadó, E. Canela, The Endocannabinoid System as a Target in Cancer Diseases: Are We There Yet? Front. Pharmacol. 10 (2019) 339, eCollection 2019.

[7] R.G. Pertwee, Pharmacological actions of cannabinoids. Handb. Exp. Pharmacol. 2005, 1–51.

[8] L. De Petrocellis, V. Di Marzo, An introduction to the endocannabinoid system: from the early to the latest concepts. Best Pract. Res. Clin. Endocrinol. Metab. 2009, 23, 1–15.

[9] G. Navarro, P. Morales, C. Rodríguez-Cueto, J. Fernández-Ruiz, N. Jagerovic, R. Franco, Targeting cannabinoid CB2 receptors in the central nervous system. Medicinal chemistry approaches with focus on neurodegenerative disorders. Front. Neurosci. 2016, 10, 406.

[10] D. Boche, V. H. Perry, J. A. Nicoll, Review: activation patterns of microglia and their identification in the human brain. Neuropathol. Appl. Neurobiol. 39 (2013) 3–18.

[11] E. Aso, I. Ferrer, CB2 cannabinoid receptor as potential target against Alzheimer's disease. Front. Neurosci. 10 (2016) 243.

[12] E. Aso, S. Juvés, R. Maldonado, I. Ferrer, CB2 cannabinoid receptor agonist ameliorates Alzheimer-like phenotype in AβPP/PS1 mice. J. Alzheimer's Dis. 35 (2013) 847–858.

[13] J. Wu, B. Bie, H. Yang, J.J. Xu, D. L. Brown, M. Naguib, Activation of the CB2 receptor system reverses amyloid-induced memory deficiency. Neurobiol. Aging 34 (2013) 791–804.

[14] A.M. Martín-Moreno, B. Brera, C. Spuch, E. Carro, L. García-García, M. Delgado, M. A. Pozo, N. G. Innamorato, A. Cuadrado, M. L. de Ceballos, Prolonged oral cannabinoid administration prevents neuroinflammation, lowers β-amyloid levels and improves cognitive performance in Tg APP 2576 mice. J. Neuroinflammation 9 (2012) 8.

[15] M. Pyszniak, J. Tabarkiewicz, J. J. Łuszczki, Endocannabinoid system as a regulator of tumor cell malignancy - biological pathways and clinical significance. Onco. Targets Ther. 9 (2016) 4323–4336.

[16] E.L. Scotter, M. E. Abood, M. Glass, The endocannabinoid system as a target for the treatment of neurodegenerative disease. Br. J. Pharmacol. 160 (2010) 480–498.

[17] T. Bisogno, S. Oddi, A. Piccoli, D. Fazio, M. Maccarrone, Type-2 cannabinoid receptors in neurodegeneration. Pharmacol Res. 111 (2016) 721–730.

[18) T. Kisková, F. Mungenast, M. Suváková, W. Jäger, T. Thalhammer, Future Aspects for Cannabinoids in Breast Cancer Therapy. Int. J. Mol. Sci. 20 (2019) 1673.

[19] M. Rao, D. Chen, P. Zhan, J. Jiang, MDA19, a novel CB2 agonist, inhibits hepatocellular carcinoma partly through inactivation of AKT signaling pathway. Biol Direct. 14 (2019) 9.

[20] F. Punzo, C. Tortora, D. Di Pinto, I. Manzo, G. Bellini, F. Casale, F. Rossi, Anti-proliferative, pro-apoptotic and anti-invasive effect of EC/EV system in human osteosarcoma. Oncotarget 8 (2017) 54459–54471.

[21] F. Punzo, I. Manzo, C. Tortora, E. Pota, V. Angelo, G. Bellini, A. Di Paola, F. Verace, F. Casale, F. Rossi, Effects of CB2 and TRPV1 receptors' stimulation in pediatric acute T-lymphoblastic leukemia. Oncotarget 9 (2018) 21244–21258.

[22] A. Bettiga, M. Aureli, G. Colciago, V. Murdica, M. Moschini, R. Lucianò, D. Canals, Y. Hannun, P. Hedlund, G. Lavorgna, R. Colombo, R. Bassi, M. Samarani, F. Montorsi, A. Salonia, F. Benigni, Bladder cancer cell growth and motility implicate cannabinoid 2 receptor-mediated modifications of sphingolipids metabolism. Sci. Rep. 7 (2017) 42157.

[23] G. Velasco, C. Sanchez, M. Guzman, Towards the use of cannabinoids as antitumour agents. Nat. Rev. Cancer 12 (2012) 436–444.

[24] C. Blazquez, A. Carracedo, L. Barrado, P.J. Real, J. L. Fernandez-Luna, G. Velasco, M. Malumbres, M. Guzman, Cannabinoid receptors as novel targets for the treatment of melanoma. FASEB J. 20 (2006) 2633–2635.

[25] Z. Qamri, A. Preet, M. W. Nasser, C. E. Bass, G. Leone, S. H. Barsky, R. K. Ganju, Synthetic cannabinoid receptor agonists inhibit tumor growth and metastasis of breast cancer. Mol. Cancer Ther. 8 (2009) 3117–3129.

[26] S. Sarfaraz, F. Afaq, V. M. Adhami, A. Malik, H. Mukhtar, Cannabinoid receptor agonist-induced apoptosis of human prostate cancer cells LNCaP proceeds through sustained activation of ERK1/2 leading to G1 cell cycle arrest. J. Biol. Chem. 281 (2006) 39480–39491.

[27] B. K. Atwood, K. Mackie, CB2: a cannabinoid receptor with an identity crisis. Br. J. Pharmacol. 160 (2010) 467–479.

[28] A. M. Malfitano, S. Basu, K. Maresz, M. Bifulco, B. N. Dittel, What we know and do not know about the cannabinoid receptor 2 (CB2), Semin. Immunol. 26 (2014) 369–379.

[29] A. M. Tabrizi, P.G. Baraldi, P.A. Borea, K. Varani, Medical chemistry, pharmacology and potential therapeutic benefits of cannabinoid CB2receptor agonists, Chem. Rev. 116 (2016) 519–560.

[30] A. Franklin, S. Parmentier-Batteur, L. Walter, D. A. Greenberg, N. Stella, Palmitoylethanolamide increases after focal cerebral ischemia andpotentiates microglial cell motility. J. Neurosci. 23 (2003) 7767–7775.

[31] M. T. Viscomi, S. Oddi, L. Latini, N. Pasquariello, F. Florenzano, G. Bernardi, M. Molinari, M. Maccarrone, Selective CB2 receptor agonism protects centralneurons from remote axotomy-induced apoptosis through the PI3K/Aktpathway, J. Neurosci. 29 (2009) 4564–4570.

[32] F. S. den Boon, P. Chameau, Q. Schaafsma-Zhao, W. van Aken, M. Bari, S. Oddi, C. G. Kruse, M. Maccarrone, W. J. Wadman, T. R. Werkman, Excitability of prefrontal cortical pyramidal neurons is

modulated by activation of intracellular type-2 cannabinoid receptors, Proc. Natl. Acad. Sci. U. S. A. 109 (2012) 3534–3539.

[33] S. Oddi, L. Latini, M. T. Viscomi, E. Bisicchia, M. Molinari, M. Maccarrone, Distinct regulation of nNOS and iNOS by CB2receptor in remote delayedneurodegeneration, J. Mol. Med. 90 (2012) 371–387.

[34] S. R. Smith, C. Terminelli, G. Denhardt, Effects of cannabinoid receptor agonist and antagonist ligands on production of inflammatory cytokines and anti-inflammatory interleukin-10 in endotoxemic mice, J. Pharmacol. Exp.Ther. 293 (2000) 136–150.

[35] F. Molina-Holgado, E. Pinteaux, J. D. Moore, E. Molina-Holgado, C. Guaza, R. M. Gibson, N. J. Rothwell, Endogenous interleukin-1 receptor antagonistmediates anti-inflammatory and neuroprotective actions of cannabinoids inneurons and glia, J. Neurosci. 23 (2003) 6470–6474.

[36] N. Evens, B. Bosier, B. J. Lavey, J. A. Kozlowski, P. Vermaelen, I. Baudemprez, R. Busson, D. M. Lambert, K. Van Laere, A. M. Verbruggen, G. M. Bormans, Labelling and biological evaluation of [(11)C]methoxy-Sch225336: A radioligand for the cannabinoid-type 2 receptor. Nucl. Med. Biol. 35 (2008) 793–800.

[37] N. Evens, G. G. Muccioli, N. Houbrechts, D. M. Lambert, A. M. Verbruggen, K. Van Laere, G. M. Bormans, Synthesis and biological evaluation of carbon-11- and fluorine-18-labeled 2-oxoquinoline derivatives for type 2 cannabinoid receptor positron emission tomography imaging. Nucl. Med. Biol. 36 (2009) 455–465.

[38] M. Gao, M. Wang, K. D. Miller, G. D. Hutchins, Q. H. Zheng, Synthesis and in vitro biological evaluation of carbon-11-labeled quinoline derivatives as new candidate PET radioligands for cannabinoid CB2 receptor imaging. Bioorg. Med. Chem. 18 (2010) 2099–2106.

[39] N. Turkman, A. Shavrin, V. Paolillo, H. H. Yeh, L. Flores, S. Soghomonian, B. Rabinovich, A. Volgin, J. Gelovani, M. Alauddin, Synthesis and preliminary evaluation of [18F]-labeled 2-oxoquinoline derivatives for PET imaging of cannabinoid CB2 receptor. Nucl. Med. Biol. 39 (2012) 593–600.

[40] B. C. Boekhorst, S. M. Bovens, J. Rodrigues-Feo, H. M. Sanders, C. W. van de Kolk, A. I. de Kroon, M. J. Cramer, P. A. Doevendans, M. ten Hove, G. Pasterkamp, C. J. van Echteld, Characterization and in

vitro and in vivo testing of CB2-receptor- and NGAL-targeted paramagnetic micelles for molecular MRI of vulnerable atherosclerotic plaque. Mol. Imaging Biol. 12 (2010) 635-651.

[41] R. Cilia, Molecular Imaging of the Cannabinoid System in Idiopathic Parkinson's Disease. Int Rev Neurobiol. 141 (2018) 305–345.

[42] J. C. McGrath, S. Arribas, C. J. Daly, Fluorescent Ligands for the Study of Receptors. Trends Pharmacol. Sci. 17 (1996) 393–399.

[43] A. S. Yates, S. W. Doughty, D. A. Kendall, B. Kellam, Chemical Modification of the Naphthoyl 3-Position of JWH-015: In Search of a Fluorescent Probe to the Cannabinoid CB2 Receptor. Bioorg. Med. Chem. Lett. 15 (2005) 3758–3762.

[44] V. M. Showalter, D. R. Compton, B. R. Martin, M. E. Abood, Evaluation of Binding in a Transfected Cell Line Expressing a Peripheral Cannabinoid Receptor (CB2): Identification of Cannabinoid Receptor Subtype Selective Ligands. J. Pharmacol. Exp. Ther. 178 (1996) 989 LP–999.

[45] R. R. Petrov, M. E. Ferrini, Z. Jaffar, C. M. Thompson, K. Roberts, P. Diaz, Design and Evaluation of a Novel Fluorescent CB2 Ligand as Probe for Receptor Visualization in Immune Cells. Bioorg. Med. Chem. Lett. 21 (2011) 5859–5862.

[46] I. Martinić, S. V. Eliseeva, S. Petoud, Near-Infrared Emitting Probes for Biological Imaging: Organic Fluorophores, Quantum Dots, Fluorescent Proteins, Lanthanide(III) Complexes and Nanomaterials J. Lumin. 189 (2017) 19–43.

[47] M. Rinaldi-Carmona, F. Barth, J. Millan, J. M. Derocq, P. Casellas, C. Congy, D. Oustric, M. Sarran, M. Bouaboula, B. Calandra, B.; M. Portier, D. Shire, J.-C. Brelière, G.Le Fur, SR144528, the First Potent and Selective Antagonist of the CB2 Cannabinoid Receptor. J. Pharmacol. Exp. Ther. 284 (1998) 644-650.

[48] M. Bai, M. Sexton, N. Stella, D. J. Bornhop, MBC94, a Conjugable Ligand for Cannabinoid CB2 Receptor Imaging. Bioconjug. Chem. 19 (2008) 988–992.

[49] M. Sexton, G. Woodruff, E. A. Horne, Y. H. Lin, G.G. Muccioli, M. Bai, E. Stern, D. J. Bornhop, N. Stella, NIR-Mbc94, a Fluorescent Ligand That Binds to Endogenous CB2 Receptors and Is Amenable to High-Throughput Screening. Chem. Biol. 18 (2011) 563–568.

[50] S. Zhang, P. Shao, M. Bai, In Vivo Type 2 Cannabinoid Receptor-Targeted Tumor Optical Imaging Using a Near Infrared Fluorescent Probe. Bioconjug. Chem. 24 (2013) 1907–1916.

[51] S. Zhang, P. Shao, X. Ling, L. Yang, W. Hou, S. H. Thorne, W. Beaino, C. J. Anderson, Y. Ding, M. Bai, In Vivo Inflammation Imaging Using a CB2RTargeted near Infrared Fluorescent Probe. Am. J. Nucl. Med. Mol. Imaging 5 (2015) 246–258.

[52] Z. Wu, P. Shao, S. Zhang, M. Bai, Targeted Zwitterionic near Infrared Fluorescent 125 Probe for Improved Imaging of Type 2 Cannabinoid Receptors. J. Biomed. Opt. 19 (2014) 036006.

[53] Z. Wu, P. Shao, S. Zhang, X. Ling, M. Bai, Molecular Imaging of Human Tumor Cells That Naturally Overexpress Type 2 Cannabinoid Receptors Using a Quinolone-Based near-Infrared Fluorescent Probe. J. Biomed. Opt. 19 (2014) 76016.

[54] X. Ling, S. Zhang, P. Shao, W. Li, L. Yang, Y. Ding, C. Xu, N. Stella, M. Bai, A Novel Near-Infrared Fluorescence Imaging Probe That Preferentially Binds to Cannabinoid Receptors CB2R over CB1R. Biomaterials 57 (2015) 169–178.

[55] X. Guo, X. Ling, F. Du, Q. Wang, W. Huang, Z. Wang, X. Ding, M. Bai, Z. Wu, Molecular Imaging of Pancreatic Duct Adenocarcinoma Using a Type 2 Cannabinoid Receptor-Targeted Near-Infrared Fluorescent Probe. Transl. Oncol. 11 (2018) 1065–1073.

[56] E. Stern, G. G. Muccioli, R. Millet, J. F. Goossens, A. Farce, P. Chavatte, J. H. Poupaert, D. M. Lambert, P. Depreux, J. P. Hénichart, Novel 4-Oxo-1,4-Dihydroquinoline-3-Carboxamide Derivatives as New CB2 Cannabinoid Receptors Agonists: Synthesis, Pharmacological Properties and Molecular Modeling. J. Med. Chem. 49 (2006) 70–79.

[57] S. Pasquini, L. Botta, T. Semeraro, C. Mugnaini, A. Ligresti, E. Palazzo, S. Maione, V. DiMarzo, F. Corelli, Investigations on the 4-Quinolone-3-Carboxylic Acid Motif. 2. Synthesis and Structure−Activity Relationship of Potent and Selective Cannabinoid-2 Receptor Agonists Endowed with Analgesic Activity in Vivo. J. Med. Chem. 51 (2008) 5075–5084.

[58] C. Abate, M. Niso, R. Marottoli, C. Riganti, D. Ghigo, S. Ferorelli, G. Ossato, R. Perrone, E. Lacivita, D. C. Lamb, F. Berardi, Novel derivatives of 1-cyclohexyl-4-[3-(5-methoxy-1,2,3,4-tetrahydronaphthalen-1-

yl)propyl]piperazine (PB28) with improved fluorescent and σ receptors binding properties. J. Med. Chem. 57 (2014) 3314–3323.

[59] M. Niso, C. Riganti, M. L. Pati, D. Ghigo, F. Berardi, C. Abate, Novel and Selective Fluorescent σ2 - Receptor Ligand with a 3,4-Dihydroisoquinolin-1-one Scaffold: A Tool to Study σ2 Receptors in Living Cells. ChemBioChem 16 (2015) 1078–83.

[60] C. Abate, C. Riganti, M. L. Pati, D. Ghigo, F. Berardi, T. Mavlyutov, L. W. Guo, A. Ruoho, Development of sigma-1 (σ1) receptor fluorescent ligands as versatile tools to study σ1 receptors. Eur J Med Chem. 108 (2016) 577–585.

[61] A. Scilimati, S. Ferorelli, M. C. Iaselli, M. Miciaccia, M. L. Pati, C. G. Fortuna, A. M. Aleem, L. J. Marnett, M. G. Perrone, Targeting COX-1 by mofezolac-based fluorescent probes for ovarian cancer detection. Eur. J. Med. Chem. 179 (2019) 16–25.

[62] S. Pasquini, S.; De Rosa, M. A. Ligresti, C. Mugnaini, A. Brizzi, N. P. Caradonna, M. G. Cascio, D. Bolognini, R. G. Pertwee, V. Di Marzo, F. Corelli, Investigations on the 4-Quinolone-3-Carboxylic Acid Motif. 6. Synthesis and Pharmacological Evaluation of 7-Substituted Quinolone-3-Carboxamide Derivatives as High Affinity Ligands for Cannabinoid Receptors. Eur. J. Med. Chem. 58 (2012) 30–43.

[63] B. Pal, P. Jaisankar, V. S. Giri, Versatile Reagent for Reduction of Azides to Amines. Synth. Commun. 34 (2004) 1317–1323.

[64] M. Sainlos, B. Imperiali, Synthesis of Anhydride Precursors of the Environment-Sensitive Fluorophores 4-DMAP and 6-DMN. Nat. Protoc. 2 (2007) 3219-3225.

[65] M. Leopoldo, E. Lacivita, F. Berardi, R. Perrone, Developments in Fluorescent Probes for Receptor Research. *Drug Discov. Today* 2009, *14 (13-14)*, 706–-712.

[66] K. J. Valenzano, L. Tafesse, G. Lee, J. E. Harrison, J. M. Boulet, S. L. Gottshall, L. Mark, M. S. Pearson, W. Miller, S. Shan, L. Rabadi, Y. Rotshteyn, S. M. Chaffer, P. I. Turchin, D. A. Elsemore, M. Toth, L. Koetzner, G. T. Whiteside, Pharmacological and Pharmacokinetic Characterization of the Cannabinoid Receptor 2 Agonist, GW405833, Utilizing Rodent Models of Acute and Chronic Pain, Anxiety, Ataxia and Catalepsy. Neuropharmacology 48 (2005) 658–672.

[67] D. Roberto, L. H. Klotz, V. Venkateswaran, Cannabinoid WIN 55,212-2 induces cell cycle arrest and apoptosis, and inhibits proliferation, migration, invasion, and tumor growth in prostate cancer in a cannabinoid-receptor 2 dependent manner. Prostate 79 (2019) 151–159.

[68] N. Olea-Herrero, D. Vara, S. Malagarie-Cazenave, I. Díaz-Laviada, Inhibition of human tumour prostate PC-3 cell growth by cannabinoids R(+)-Methanandamide and JWH-015: involvement of CB2. Br J Cancer. 101 (2009) 940–950.

[69] S. Sarfaraz, F. Afaq, V. M. Adhami, H. Mukhtar, Cannabinoid receptor as a novel target for the treatment of prostate cancer. Cancer Res. 65 (2005) 1635-1641.

[70] I. Dando, M. Donadelli, C. Costanzo, E. Dalla Pozza, A. D'Alessandro, L. Zolla, M. Palmieri, Cannabinoids inhibit energetic metabolism and induce AMPK-dependent autophagy in pancreatic cancer cells. Cell Death Dis. 2013, 4, e664.

[71] A. Carracedo, M. Gironella, M. Lorente, S. Garcia, M. Guzmán, G. Velasco, J. L. Iovanna, Cannabinoids induce apoptosis of pancreatic tumor cells via endoplasmic reticulum stress-related genes. Cancer Res. 66 (2006) 6748–6755.

[72] W. Tuo, M. Bollier, N. Leleu-Chavain, L. Lemaire, A. Barczyk, X. Dezitter, F. Klupsch, F. Szczepanski, J. Spencer, P. Chavatte, R. Millet, Development of novel oxazolo[5,4-d]pyrimidines as competitive CB_2 neutral antagonists based on scaffold hopping. Eur. J. Med. Chem. 146 (2018) 68–78.

[73] M. Linsalata, M. Notarnicola, V. Tutino, M. Bifulco, A. Santoro, C. Laezza, C. Messa, A. Orlando, M. G. Caruso, Effects of anandamide on polyamine levels and cell growth in human colon cancer cells. Anticancer Res. 30 (2010) 2583–2589.

[74] S. Sreevalsan, S. Safe, The cannabinoid WIN 55,212-2 decreases specificity protein transcription factors and the oncogenic cap protein eIF4E in colon cancer cells. Mol Cancer Ther. 12 (2013) 2483–2493.

[75] C. Riganti, E. Miraglia, D. Viarisio, C. Costamagna, G. Pescarmona, D. Ghigo, A. Bosia, Nitric oxide reverts the resistance to doxorubicin in human colon cancer cells by inhibiting the drug efflux. Cancer Res. 65 (2005) 516–525.

[76] I. Pedrini, E. Gazzano, K. Chegaev, B. Rolando, A. Marengo, J. Kopecka, R. Fruttero, D. Ghigo, S. Arpicco, C. Riganti, Liposomal nitrooxy-doxorubicin: one step over caelyx in drug-resistant human cancer cells. Mol Pharm. 11 (2014) 3068–3079.

[77] K. E. Hanlon, A. N. Lozano-Ondoua, P. J. Umaretiya, A.M. Symons-Liguori, A. Chandramouli, J. K. Moy, W. K. Kwass, P. W. Mantyh, M. A. Nelson, T. W. Vanderah, Modulation of breast cancer cell viability by a cannabinoid receptor 2 agonist, JWH-015, is calcium dependent. Breast Cancer 8 (2016) 59–71

[78] Blasco-Benito, S.; Moreno, E.; Seijo-Vila, M.; Tundidor, I.; Andradas, C.; Caffarel, M.M.; Caro-Villalobos, M.; Urigüen, L.; Diez-Alarcia, R.; Moreno-Bueno, G.; Hernández, L.; Manso, L.; Homar-Ruano, P.; McCormick, P.J.; Bibic, L.; Bernadó-Morales, C.; Arribas, J.; Canals, M.; Casadó, V.; Canela, E.I.; Guzmán, M.; Pérez-Gómez, E.; Sánchez, C. Therapeutic targeting of HER2-CB2R heteromers in HER2-positive breast cancer. *Proc Natl Acad Sci U S A* **2019**, *116*, 3863–3872.

[79] X. Li, T. Hua, K. Vemuri, J. H. Ho, Y. Wu, L. Wu, P. Popov, O. Benchama, N. Zvonok, K. Locke, L. Qu, G. W. Han, M. R. Iyer, R. Cinar, N. J. Coffey, J. Wang, M. Wu, V. Katritch, S. Zhao, G. Kunos, L. M. Bohn, A. Makriyannis, R. C. Stevens, Z. J. Liu, Crystal Structure of the Human Cannabinoid Receptor CB2. Cell 176 (2019) 459–467.

[80] S. Tsuzuki, K. Honda, T. Uchimaru, M. Mikami, Intermolecular interactions of nitrobenzene-benzene complex and nitrobenzene dimer: Significant stabilization of slipped-parallel orientation by dispersion interaction J. Chem. Phys. 125 (2006) 124304.

[81] C. Hess, C. T. Schoeder, T. Pillaiyar, B. Madea, C. E. Müller, Pharmacological evaluation of synthetic cannabinoids identified as constituents of spice. Forensic Toxicol. 34 (2016) 329-343.

[82] N.A. Colabufo, F. Berardi, M. Contino, M. Niso, C. Abate, R. Perrone, V. Tortorella, Antiproliferative and cytotoxic effects of some σ_2 agonists and σ_1 antagonists in tumour cell lines. Naunyn-Schmiedeberg's Arch Pharmacol. 370 (2004) 106–113.

[83] J. Kopecka, I. Campia, A. Jacobs, A.P. Frei, D. Ghigo, B. Wollscheid, Carbonic anhydrase XII is a new therapeutic target to overcome chemoresistance in cancer cells. Oncotarget 6 (2015) 6776–6793.

[84] Schrödinger Release 2018-4: Schrödinger Suite 2018-4 Protein Preparation Wizard; Epik, Schrödinger, LLC, New York, NY, 2016; Impact, Schrödinger, LLC, New York, NY, 2016; Prime, Schrödinger, LLC, New York, NY, 2018.

[85] Schrödinger Release 2018-4: LigPrep, Schrödinger, LLC, New York, NY, 2018) (Schrödinger Suite 2018-4.

[86] R. A. Friesner, R. B. Murphy, M. P. Repasky, L. L. Frye, J. R. Greenwood, T. A. Halgren, P. C. Sanschagrin, D. T. Mainz, Extra Precision Glide: Docking and Scoring Incorporating a Model of Hydrophobic Enclosure for Protein−Ligand Complexes. J. Med. Chem. 49 (2006) 6177–6196.

[87] J. L. Banks, H. S. Beard, Y. Cao, A. E. Cho, W. Damm, R. Farid, A. K. Felts, T. A. Halgren, D. T. Mainz, J. R. Maple, R. Murphy, D. M. Philipp, M. P. Repasky, L. Y. Zhang, B. J. Berne, R. A. Friesner, E. Gallicchio, R. M. Levy, Integrated Modeling Program, Applied Chemical Theory (IMPACT). J. Comput. Chem. 26 (2005) 1752–1780.

Graphical Abstracts